ISTITUTO NAZIONALE DI FISICA NUCLEARE - ISTITUTO NAZIONALE DI FISICA NUCLEARE - ISTITUTO NAZIONALE DI FISICA NUCLEARE - ISTITUTO NAZIONALE DI FISICA NUCLEARE - ISTITUTO NAZIONALE DI FISICA NUCLEARE - ISTITUTO NAZIONALE DI FISICA NUCLEARE - ISTITUTO NAZIONALE DI

Laboratori Nazionali di Frascati

LNF-90/084 (R)
5 Dicembre 1990

BGO Collaboration:

THE BGO COLLABORATION PROGRESS REPORT 1990

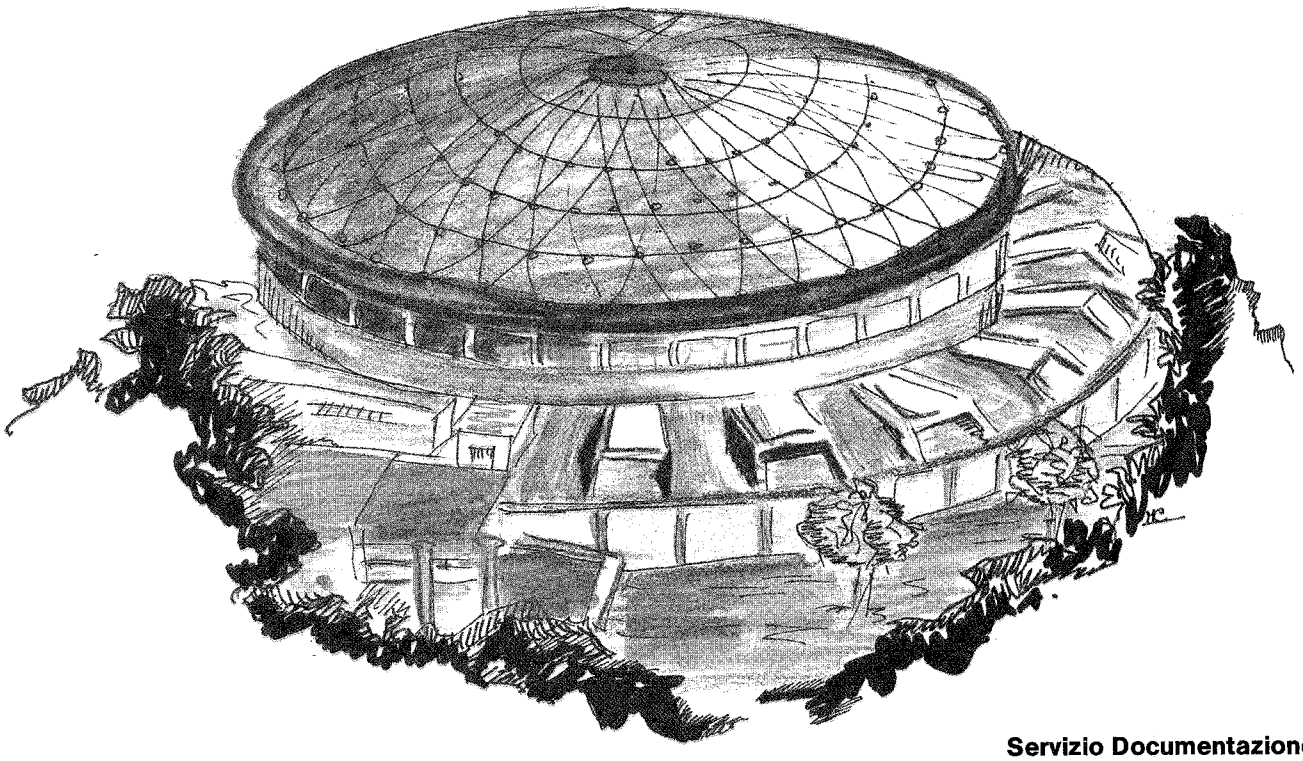

Servizio Documentazione
dei Laboratori Nazionali di Frascati
P.O. Box, 13 - 00044 Frascati (Italy)

INFN - Laboratori Nazionali di Frascati
Servizio Documentazione

LNF-90/084(R)
5 Dicembre 1990

THE BGO COLLABORATION PROGRESS REPORT 1990

RESEARCH COLLABORATORS:
M. Anghinolfi[1], D. Babusci[2], V. Bellini[3], N. Bianchi[2], L. Casano[4], P. Corvisiero[1], A. D'Angelo[4], E. De Sanctis[2], S. Frullani[5], F. Garibaldi[5], G. Gervino[6], B. Girolami[5], P. Levi Sandri[2], V. Lucherini[2], L. Mazzaschi[1], V. Muccifora[2], P. Picozza[4], E. Polli[2], A.R. Reolon[2], G. Ricco[1], M. Ripani[1], P. Rossi[5], M. Sanzone[1], C. Schaerf[4], M.L.Sperduto[3], M. Taiuti[1], G.M.Urciuoli[5] and A. Zucchiatti[1].

TECHNICAL STAFF:
M. Albicocco[2], M. Castoldi[1], E. Cima[2], E. Durante[1], L. Falco[2], G. Giuliano[1], M. Iannarelli[2], A. Macioce[2], G. Nobili[4], A. Orlandi[2], F. Parodi[1], W. Pesci[2], E. Turri[2], A. Rottura[1] and A. Viticchié[2].

1 *Istituto Nazionale di Fisica Nucleare and Dipartimento di Fisica della Università, Genova-Italy.*
2 *Istituto Nazionale di Fisica Nucleare - Laboratori Nazionali di Frascati-Italy.*
3 *Istituto Nazionale di Fisica Nucleare Laboratori Nazionali del Sud and Dipartimento di Fisica dell' Università, Catania-Italy.*
4 *Istituto Nazionale di Fisica Nucleare and Dipartimento di Fisica della Seconda Università, Roma -Italy.*
5 *Istituto Nazionale di Fisica Nucleare Istituto Superiore di Sanità, Roma-Italy.*
6 *Istituto Nazionale di Fisica Nucleare and Dipartimento di Fisica Sperimentale della Università, Torino-Italy.*

ABSTRACT

A large solid angle BGO calorimeter is under construction for photonuclear experiments at intermediate energy facilities. In this note the status progress of the project, the technical steps undertaken in the construction of the apparatus and the goals of this initiative are reviewed.

1. INTRODUCTION

The availability of high duty-cycle intermediate energy electron and photon beams in the very near future opens interesting and exciting possibilities in the study of nuclear reactions. The energy of these beams, some of which are already existing (JET TARGET in Frascati, LEGS in Brookhaven, MAMI-B in Mainz, ELSA in Bonn) while others are under construction (CEBAF in Newport News, GRAAL in Grenoble .....), covers the range that roughly goes from the pion production threshold to the energy where the Bjiorken scaling shows up, which is mainly the region where neither the conventional nuclear physics description (nucleon + deltas + exchanged pions) nor the perturbative QCD approach (quarks and gluons + exchanged gluons) hold.

From the experimental point of view this interesting and complex energy region can be tackled with two different, and in some way complementary, philosophies. The first one asks for measurements of well defined exclusive channels by means of high resolution detectors: it generally deals with little solid angles and low counting rates and brings information mainly on single particle properties of nucleons inside the nuclear medium. This philosophy proposes, in some way, the continuation of the electron scattering experimental work performed up to now at machines like the Saclay ALS and NIKHEF-K with the improvement of higher incident energy and larger duty-factor that will both allow precision measurements of form factors (at higher transferred momentum) and an easiest transverse versus longitudinal separation of response functions. On the other hand, new exotic phenomena linked to short range correlations (six-quarks bags, dibaryon resonances, signals of quark-gluon plasma) and new research fields (i.e. meson-meson scattering) can be more easily investigated, as a first step, with large solid angle, medium resolution multi-purpose detectors. In that case, emphasis will be put on pioneering work on multi particle final states produced after the absorption of a high energy photon by a nucleus , a field in which the theoretical and experimental information is mostly qualitative. A 4π detector will allow measurements of very low cross sections (below 1 nb) and the possibility of detecting complete events will open exciting windows in this still badly understood field of research.

Following this latter philosophy, a large solid angle BGO calorimeter is under construction with the financial support of the Istituto Nazionale di Fisica Nucleare (INFN) [1]. The calorimeter will detect electromagnetic showers and, to some extent, charged hadrons. The instrument was designed to achieve typical crystal ball performances (large solid angle, simultaneous multiparameter measurements, good detection efficiency for neutral products like γ, π^0, η) while having some peculiar features (modularity, limited number of sectors, relatively small size). As a large solid angle electromagnetic calorimeter, the *Rugby Ball* is the ideal instrument for the detection of photons and of

neutral mesons decaying into the two (or more) photon channel (π^0, η, K_S^0,...). The calorimeter can also detect protons, with reasonable energy resolution, up to an energy of $\approx$ 300 MeV. At higher kinetic energy the nuclear interaction becomes appreciable and the energy response displays a low energy tail. This limitation is even more true when the detection of charged pions or kaons is considered. Therefore the *Rugby Ball* should work in connection with beams of known energy (tagged photon beams). The symmetry of this detector with respect to the azimuthal angle will make it the ideal companion to polarized beams and/or polarized targets for the measurements of polarization asymmetries which could be practically free of systematic errors.

The design has taken into consideration a constant thickness of 24 cm (21 r.l.) in every (ϑ,φ) direction, a reasonable angular resolution (compatibly with the limited number of sectors) and the confinement of photon showers up to 2 GeV. The resulting structure is made of 480 pyramidal crystals, 15 in the ϑ-plane by 32 in the φ-plane. Angles from 25° to 155° are covered to a $\Delta\Omega$ = 11.3 sr. The crystals are manufactured and surface treated by Enghelard B.V. to produce a good longitudinal uniformity. When tested with a Cesium γ-source (E_γ = 661 keV) the crystals showed an overall peak spread below 5% associated with an average energy resolution of 18%. The uniformity and resolution will be controlled, for all crystals, by an automatic scanner of original design.

The BGO temperature related drifts will be corrected according to the measured light efficiency variation [2]. A gain monitoring procedure using a Xenon lamp will control the stability. As assessed on a few samples the linearity and stability (time and temperature related) of photomultipliers should be achieved up to I_{peak} = 100 mA which corresponds to a linearity range for the individual sectors of roughly 1.4 GeV.

The mechanical structure will consist of 24 carbon fibre baskets, containing 20 crystals each and supported by an external steel frame. The baskets, manufactured by Italcompositi, are similar to a honeycomb, since they are divided in cells to keep the crystals optically and mechanically separated. The thickness of the carbon walls is 0.38 mm (inner walls) and 0.54 mm (outer walls); in this way only a very small amounts of inert low Z material will be interposed between the reaction products and the active BGO medium. The calculation predicts a very low (< 0.19 mm) overall deformation for a loaded basket in any position. The steel support frame will give rigidity to the spectrometer and will be separable into two moving halves to give access to the center.

In order to increase the experimental possibilities offered by the *Rugby Ball*, a central detector will be hosted in the 20 cm Ø axial hole of the calorimeter. It will be used mainly for particle identification and to obtain the better charged particles angular resolution that will allow the use of long (up to 10 cm) cryogenic targets.

Montecarlo simulation has been used to predict the main features of such a device. A gamma-ray energy resolution of $\sigma(E)/E \approx 1\%$ at 1 GeV is consistently given by the

calculations that include all active and inert calorimeter components and target and vacuum-pipe effects.

2. DESCRIPTION OF THE APPARATUS

2.1. Intrinsic and instrumental effects in BGO energy resolution.

In general terms the overall energy resolution of a BGO counter can be written as:

$$\frac{\sigma(E)}{E} = \frac{1}{E}\left[\sigma_{fe}^2 + \sigma_s^2 + \sigma_{dis}^2 + \sigma_{temp}^2 + \sigma_{PM}^2 + \sigma_{en}^2\right]^{\frac{1}{2}}$$

where the contributions are:

- σ_{fe} intrinsic width due to the energy escape from the crystal boundaries,
- σ_s statistics of the primary photoelectrons,
- σ_{dis} longitudinal non uniformity,
- σ_{temp} fluctuations in emitted light induced by temperature,
- σ_{PM} intercalibration or PMT gain drifts,
- σ_{en} electronic noise,

The energy dependence of the first term will be discussed in relation to our Montecarlo simulation. It is well approximated by a relation like

$\sigma_{fe}/E = K/\sqrt{E}$ with K = 1% if E is given in GeV.

Being this term intrinsic to the process of energy release inside the BGO it should represent a lower limit to the overall resolution, approached when the other terms become all negligible. In practice, a value close to 1% above 1 GeV has been measured in a few cases [3,4].

Also the statistical contribution has an energy dependence like

$\sigma_s/E = C/\sqrt{E}$ with C = 0.3% if E is given in GeV.

C is computed assuming a conversion efficiency of 100 photoelectrons/MeV in BGO [5].

The term due to the longitudinal non uniformity, depends in principle on the energy of the primary particle with a law very difficult to determine a-priori since the effect may change from crystal to crystal. Preliminary Montecarlo calculations [1] have shown that, assuming a reproducible compensation process on every crystal, a smooth variation restricted between 0 and 10% would give $\sigma_{dis}/E < 0.6\%$. We expect to improve the uniformity to better than 5% and therefore to reduce even further this contribution. The calibration of our crystals with photons of known energy will establish if and how the effect of non uniformity changes with energy.

The effect of temperature related drifts can be estimated from the measured drift coefficients and assuming a situation where the *Rugby Ball* is thermostated within a degree. In such a case we have calculated $\sigma_{temp}/E = 0.3\%$.

The term contributed by the electronic noise should be negligible, since we use phototubes as the readout device.

The resolution value which results from our estimate of all the effects is 1.2% (in σ/E) at 1 GeV perfectly compatible with the available experimental data.

2.2. BGO crystals, characteristics and properties.

2.2.1. crystals: shape and dimensions.

The shape of the *Rugby Ball* crystals is that of a truncated pyramid with trapezoidal basis (figure 1). Each crystal, made of $Bi_4Ge_3O_{12}$ (BGO) is 24 cm long ($\approx$ 21 radiation lengths) and is wrapped up in a thin (0.03 mm) Aluminum reflector. The light output of the crystals is optically coupled to a photomultipler to produce an electric pulse. Two additional holes are provided to allow optical access to each crystal and will be used for temperature control and for light input (through optical fibres) to monitor PMT gain variations.

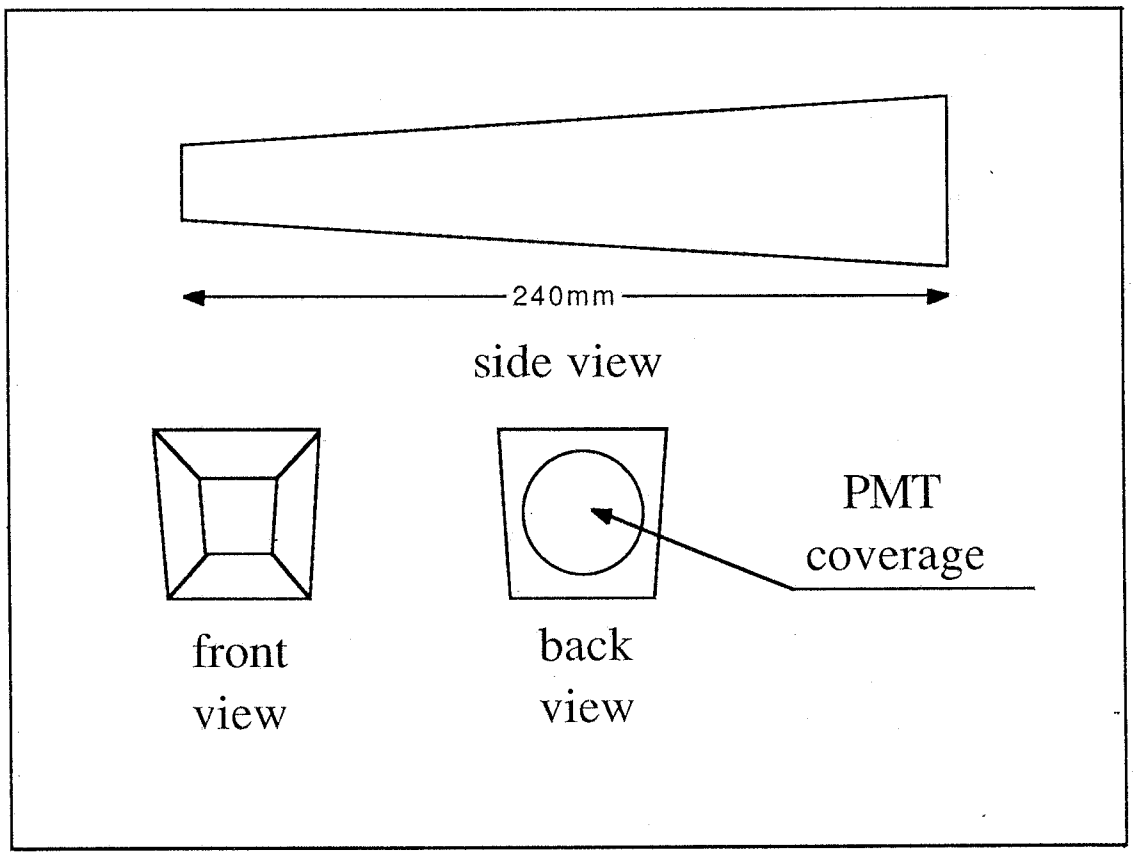

Fig. 1. *The shape of Rugby Ball BGO crystals.*

There are 8 different crystal types that differ among each other for their shapes and the dimension of their basis: in table 1 the angles subtended by each crystal type, its position in the laboratory frame and its volume are shown.

crystal type	ϑ lab [°]	$\Delta\vartheta$ lab [°]	volume [cm^3]
1	28.00 - 152.00	6.00	324.497
2	34.50 - 145.50	7.00	369.027
3	41.75 - 138.25	7.50	386.761
4	50.5 - 129.50	10.00	511.839
5	60.5 - 119.50	10.00	516.594
6	70.5 - 109.50	10.00	517.521
7	80.33 - 99.67	9.67	503.603
8	90.00	9.67	500.492

Table 1. *Crystal dimensions.*

2.2.2. Temperature behavior of a BGO prototype.

The drift with temperature of the BGO conversion efficiency is larger than that observed in NaI [6], to such an extent that it requires adequate correction (also in comparison to other effects) to avoid serious deterioration of the energy resolution obtainable. The relative spectral irradiance of BGO was measured [7] and integrated from 350 to 680 nm to give a BGO scintillation yield at six temperatures from -196°C+30°C, giving a light output variation of ≈ -1.7%/°C. A smaller gradient of -0.96% /°C was observed between 12 °C and 55 °C associated with a change in the BGO decay time of ≈ -4.7 ns/°C [5] as measured by a single photoelectron delayed coincidence. We have measured the gain and decay time variations of BGO in a temperature range from - 5 °C to + 35 °C, well representative of the ambient conditions in which our spectrometer will operate. We will recall here the main results of the tests which have already been published in detail [2]. We shall refer to the crystal bottom temperature as T1, and to the crystal top temperature as T2. A ^{137}Cs gamma source was in contact with the crystal halfway through its height. Standard anode pulse treatment has been adopted: the linearity of the entire system has been checked beforehand with several gamma sources. Since the curves start from zero, the variations of the peak position have been related directly to the variations in BGO light output. The anode pulses, induced by cosmic rays impinging on the detector are particularly suitable for the determination of the BGO decay-time because of the small statistical fluctuations on the number of photoelectrons per unit time found in these pulses as a consequence of the high energy released in BGO by cosmic events.

The peak height as a function of the crystal average temperature <T> = (T1+T2)/2, is plotted in figure 2. The experimental points are fitted in the entire temperature range by a unique straight line which corresponds to a per cent variation, relative to the 20°C point, of -1.28%/°C. The temperature drift of the photomultiplier anode sensitivity [2] was measured and resulted negligible. The decay times of cosmic-ray anode pulses, as a function of the crystal average temperature <T> are plotted in figure 3 together with the

data of reference [5]. A linear fit through all points gives a slope -5.4 ns/°C, slightly larger than that previously deduced from points in the range 12 ÷ 55 °C. The fitted line slope compares well with the measured light output variation since for exponentials of equal value at zero time and different time constants ($\tau_1 > \tau_2$) the ratio of their integrals goes like τ_1 / τ_2. In our case the peak height ratio computed for the -5 °C and the 35 °C points gives a value of 1.65, while the ratio of the fitted decay times τ_1 / τ_2 gives a value of 1.83 well within the experimental errors.

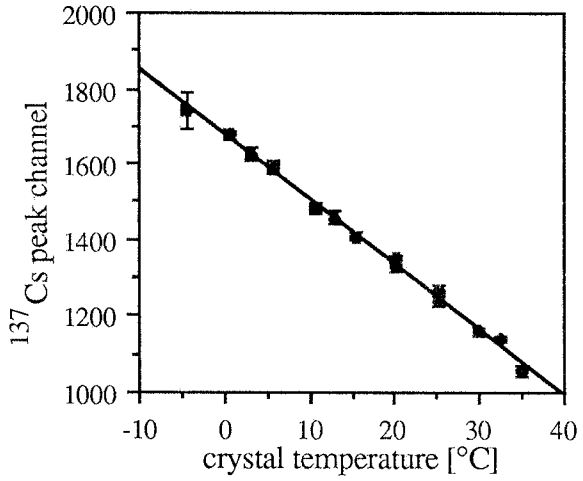

Fig. 2. *The E_γ = 661 KeV peak height variation as a function of the BGO crystal average temperature. The straight line, fitting the experimental points, corresponds to a 1.28 % variation around 20°C.*

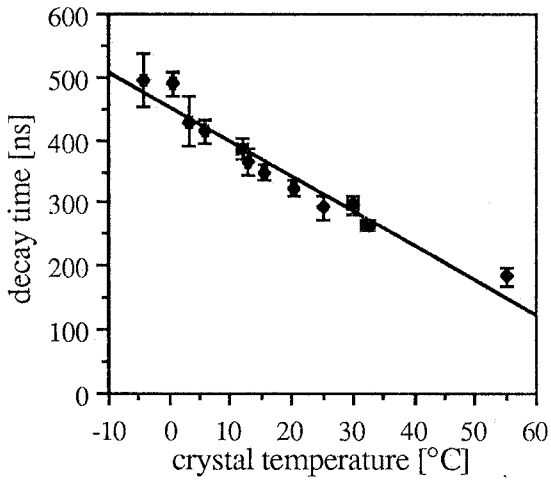

Fig. 3. *The anode pulse decay time as a function of the BGO crystal average temperature.*

These results show that the response of our BGO crystals to temperature variations is rather strong although quite slow. Therefore, to keep the temperature effect on the resolution below the contributions of the energy escape (2÷2.5% FWHM), of the expected crystal non-uniformity (less than 1.5% FWHM), and of other smaller sources (intercalibration, statistics), it is necessary to control the crystal temperature and correct accordingly, in the case of slow temperature trends. The design of the detector includes, in fact, several thermocouples conveniently positioned within the spectrometer volume . Moreover, it appears feasible and convenient to stabilize within a degree the temperature in the area in which the spectrometer will be located or at least in an area close to it, for a volume of approximately forty cubic meters.

2.2.2. The longitudinal uniformity.

The most significant instrumental contribution to the overall resolution of BGO might come from the longitudinal non uniform response induced by the BGO high refrac-

tion index (n = 2.15 at maximum emission wavelength). In order to maintain the total spectrometer energy resolution around the intrinsic value of $\sigma(E) \approx 1\%$ at E =1 GeV, indicated by the Montecarlo calculations we can tolerate a 5 % non uniformity at most. Otherwise the response of the scintillation detectors will depend not only on the energy released but also on the point of release. The effect can be explained in this way: of the total light emitted, about 70% is collected by the photocathode; one third of it suffers a partial reflection on the crystal walls, the rest being detected directly or by total reflection on the walls. For direct collection only the total reflection at the crystal-cathode interface limits the solid angle at a value $\Omega = 2\pi\ (1-\cos\vartheta_{lim})$ being $\vartheta_{lim} = \text{asin}\ (n1/n2) = 28°$. The pyramidal shape of our sectors would increase at any reflection the effective collection solid angle by an amount $\delta = 2\pi\ |\cos(\vartheta_{lim}) - \cos(\vartheta_{lim}+2\beta)|$ where β is the angle between the lateral surface and the pyramid axis. Since the number of reflections is larger for points far away from the cathode, one expects a focusing effect and large front-back non uniformities. By a Montecarlo calculation the longitudinal non uniformity of polished crystals has been computed taking into account the geometry, the light attenuation, the emission point, the concentration of air bubbles trapped inside the crystal and the total reflection on the surface [1]. The result is that the fluctuation for a pyramid inscribed in a cone of 6° can be as high as 100% (figure 4).

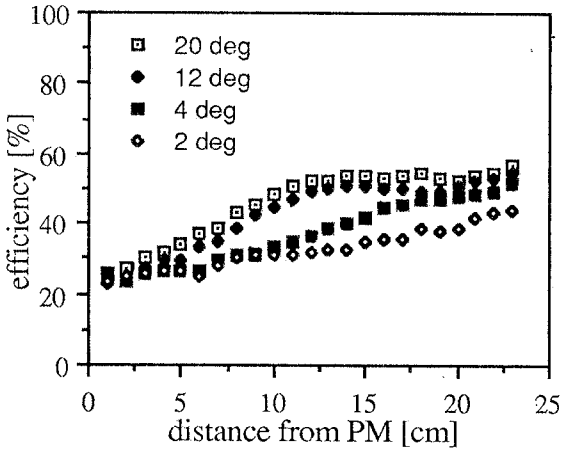

Fig. 4. *The light collection efficiency as a function of the photomultiplier distance. The different symbols show the effect of different crystal aperture angles.*

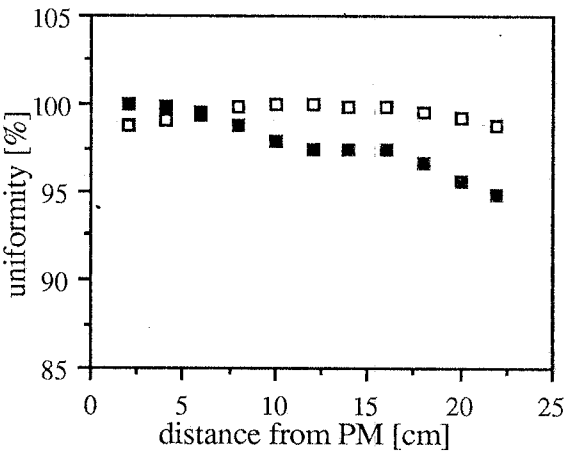

Fig. 5. *The best (open squares) and worst (full squares) uniformity patterns for light collection obtained from the first 10 delivered crystals.*

In non polished crystals the roughness of the surfaces reduces to minimum the light collected by total reflection. The amount of light collected is determined only by the attenuation process and points close to the cathode give higher responses since the distance the light has to travel is lower. The total light collected by the cathode is however appreciably smaller than for polished crystals. The two competing effects (focusing and attenuation)

are used, through an iterating process, based on partial surface treatment performed at Engelhard to deliver crystals with the required 5% maximum fluctuation. In figure 5 the results obtained by testing the first 10 delivered crystals are shown. This level of uniformity is obtained at the expenses of total collected light which implies a worsening of the resolution at ^{137}Cs up to 20% FWHM. As already explained this worsening in resolution has little effect when extrapolated to energies of relevance to our detector.

Each crystal will be treated with this compensation process and the uniformity and resolution pattern will be measured for all crystals. In order to perform this large amount of measurements, we have realized an automatic test bench of original design [8] based on a PC IBM-XT which drives the movements of the bench, performs Multi-Channel Analysis (MCA) of the BGO pulses and elaborates on-line the uniformity and resolution pattern.

The mechanical design takes into account that crystals of similar height, but different shapes, must be tested. Since gamma-rays emitted by a Cs source have a short mean free path inside the BGO, it is necessary to test the longitudinal uniformity along each face, to check if, during the growing process, some structural defects (air bubbles, crystalline plane irregularity, etc.) took place. The mechanical structure (figure 6) holds the BGO specimen vertically with the smallest base pointing downwards. The BGO is placed tightly inside a thin (0.4 mm) iron box which rotates according to pre-programmed PC commands. The Cs source, hosted in a lead collimator with a 0.5 cm Ø hole,moves up and down along the crystal sides. To keep constant the distance between the BGO surface and the collimator hole, the whole BGO supporting frame can be manually tilted with respect to the vertical line.Two stepping-motors allow the vertical movements of the radioactive source and the rotation of the crystal faces after each side scan. The step size, the translation speed, the rotation of the crystal and the measure time are all given as inputs to a PC program that executes the entire test sequence. The source position is normally incremented in steps of 2 cm. At each point a γ-ray spectrum is taken and dumped on a floppy disk. Afterwards, the acquisition program computes the FWHM, the centroid of the peak and logs them on disk. At the end of each crystal face scan, the data are retrieved and the uniformity function Ch/Ch_{MAX} (x) and FWHM(x) are computed and plotted for immediate evidence of possible departure from the agreed values of 5% for the former or 20% for the latter.

2.3. The support structure.

The *Rugby Ball* support structure is schematically represented in figure 7 where the main parts: carbon fibre baskets, iron support frame and platform, can be easily recognized. The support frame is divided into two halves, which can be taken apart by 1.5 meters sliding on precision (4 STAR) cylindrical guides. This allows access to the inner

part of the ball while insuring a highly reproducible positioning of the spectrometer. When closed, the structure has a 20 cm Ø axial hole for target insertion, beam passage and the installation of a central detector. The location of the baskets inside the structure is such that the vertical axis from the target center coincides with the axis of a crystal; therefore the two halves are tilted ≈ 6° with respect to the vertical direction.

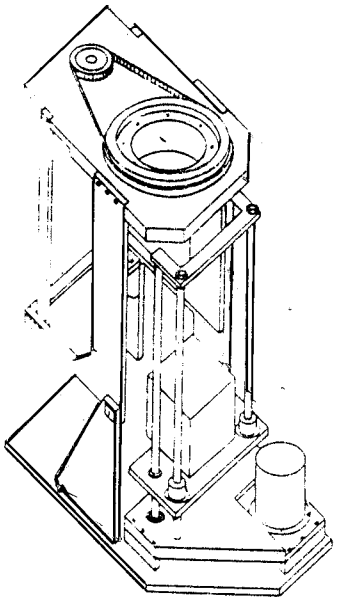

Fig. 6. *The test bench.*

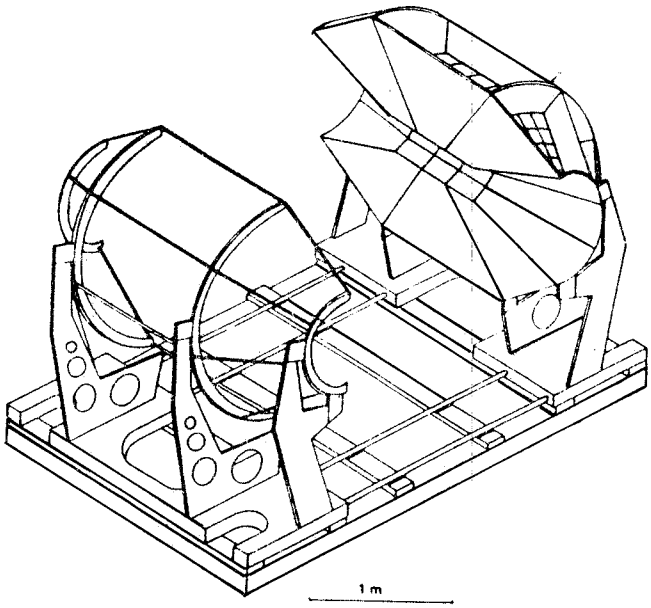

Fig. 7. *The Rugby Ball support structure.*

The platform occupies a volume of approximately 2 x 3 x 2.3 m^3 and has adjustments for planarity and beam axis matching. The height of the beam axis from the floor is supposed to be 140 cm and there is provision both for a fine (± 5 cm) adjustment of the height and for a course increase of another 30 cm by the insertion of two I-beams. The manipulation of baskets will be done by a specific tool which was designed together with the frame to fit any basket irrespective of its position in the structure.

Two preliminary studies have been commissioned to major aircraft industries concerning the realization of aluminium and carbon fibre baskets. The second option has proved much more practical in all regards. An aluminium type basket would have had a minimum thickness of 0.5 mm and a rigidity slightly lower than a carbon one. The carbon baskets (see figure 8) were designed to guarantee a maximum deformation of 0.19 mm in the corners more distant from the attack point when loaded and mounted horizontally. This is obtained with wall thicknesses of 0.38 mm for the inner walls and of 0.54 mm for the outer walls of each basket. A slightly large (≈ 1 mm) thickness is obtained at the crystal front due to unavoidable folding of the carbon tissue. In terms of gamma ray attenuation by the inert material, the carbon solution is 3 times better than the aluminium one since both the radiation length (X_0^{Al} = 89 mm, X_0^{C} = 188 mm) and the real

thickness are lower in the fibre. The baskets are produced with a co-curing technique performed in a single step. The procedure requires a specific steel tool and is patented by Agusta and Italcompositi. The steel production tools required for our baskets are of unprecedented complexity, being composed of many, large, high precision (±0.02 mm) components. Part of the structure has been completed and can give an idea of the complexity and size of the *Rugby Ball* as seen in figure 9.

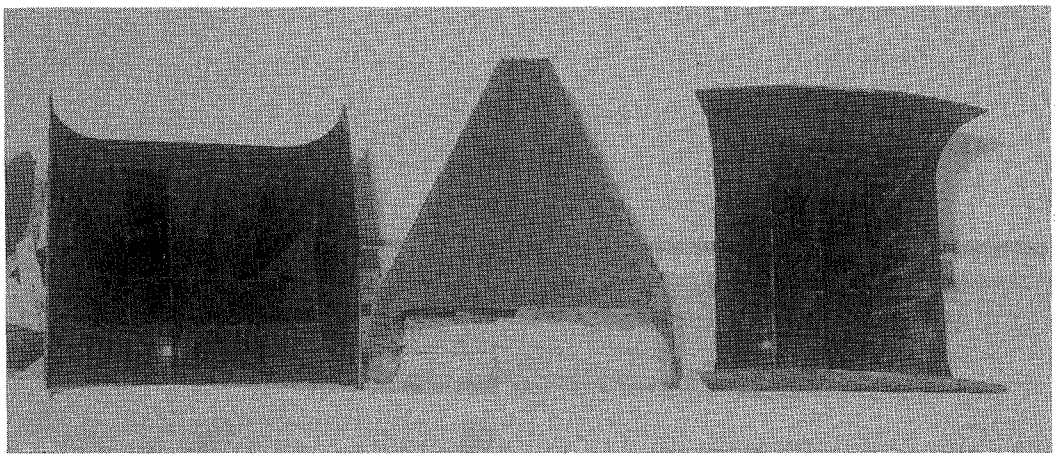

Fig. 8. *A carbon fibre basket.*

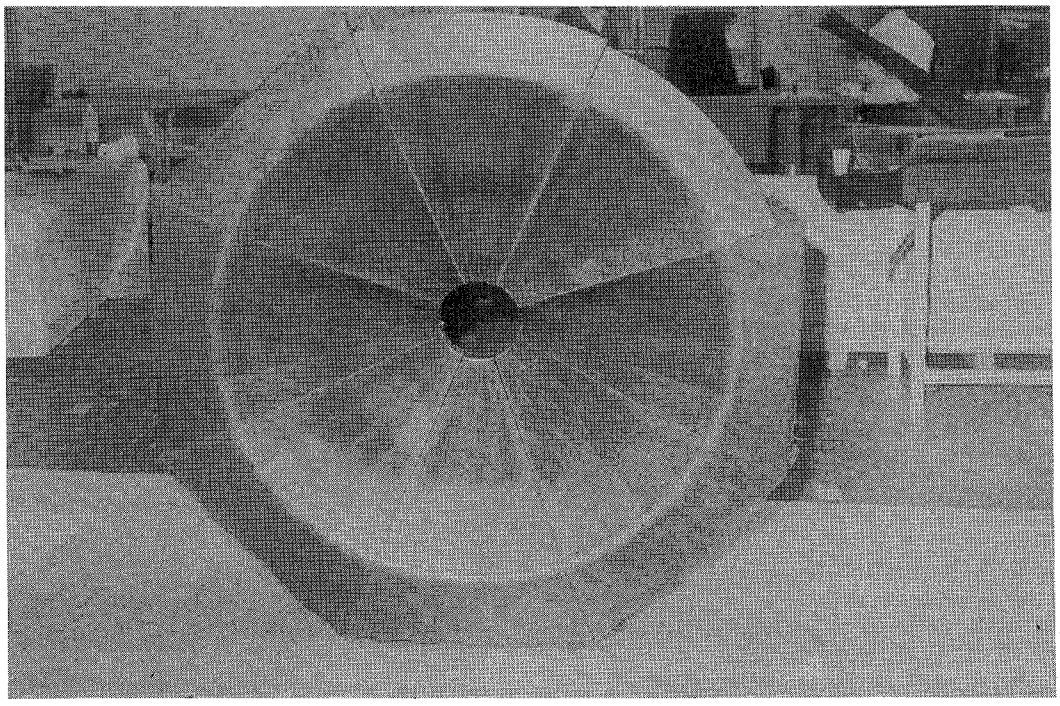

Fig. 9. A complete ring of carbon fibre baskets.

2.4. The central detector.

The *Rugby Ball* calorimeter is essentially a detector of electromagnetic showers. The possibility of recognizing with this detector showers generated by photons from those generated by electrons (positrons) and of detecting charged hadrons lies essentially

in the coupling of the *Rugby Ball* with an appropriate central equipment. The following items are to be considered in the project of such a device:

1) anticoincidence for neutral particles (essentially photons);

2) identification of protons from charged pions and electrons;

3) improvement of the angular resolution for charged particles;

4) identification of charged pions from electrons;

5) improvement of the angular resolution for photons;

The first two requirements could be satisfied by an energy loss detector, the third, by a tracking detector, the fourth and the fifth by a preshower detector.

The general layout of the central detector should be like in figure 10. Each part has an azimuthal symmetry and can be inserted and used separately inside the *Rugby Ball.* A hole of 8 cm Ø remains as a free space for cryogenic targets location.

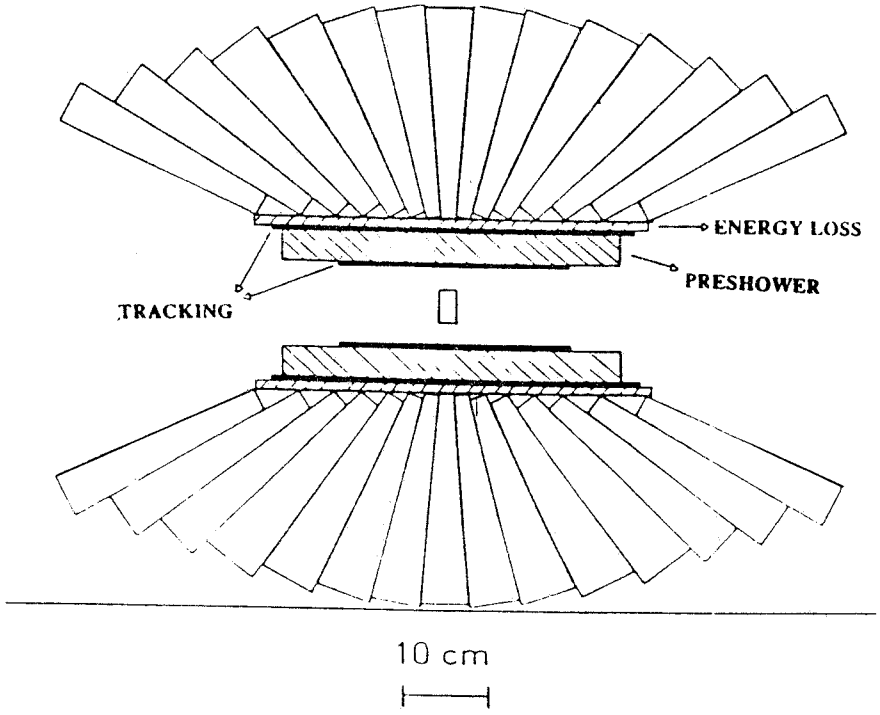

Fig. 10. *Cut view of the Rugby Ball including the general layout of the central detector.*

2.4.1. Energy loss detector.

The energy loss detector is made of a plastic cylinder (9 cm internal radius, 1 cm thickness and 45 cm length) that covers the whole internal surface of the *Rugby Ball.* This ensures that the efficiency for the detection of a charged particle is very close to 100% and that for a high energy photon close to 2%. To resolve the final state multiplicity the cylinder is segmented in 32 longitudinal sectors, viewed from both sides by two 10 stage photomultiplier. With three charged particles in the final state, with a random isotropic azimuthal distribution, the probability of 2 signals in the same sector is less than 10 %.

The energy loss detector must identify pions and electrons from protons up to ≈ 300 MeV which is the maximum hadron working energy of the *Rugby Ball*. The intrinsic energy losses for protons, pions and electrons at 300 MeV are shown in figure 11. The FWHM of the three distributions are respectively 23%, 26% and 30%. The following effects on energy losses must be minimized to optimize the proton identification:

a) Homogeneity. It has been measured on a test plastic scintillator bar of dimension 43 x 2 x 1 cm^3 viewed at both ends by two light guides and two Hamamatsu R1450 photomultipliers. Results of the test with a ^{106}Ru source are shown in figure 12 and the maximum inhomogeneity measured is about 10%.

b) Statistics. It has been measured moving the ^{106}Ru source along the scintillator bar viewed by only one photomultiplier and also using a LED; the two results give a FWHM of 20% which is less than the value of 25% expected from the measured mean anode signal.

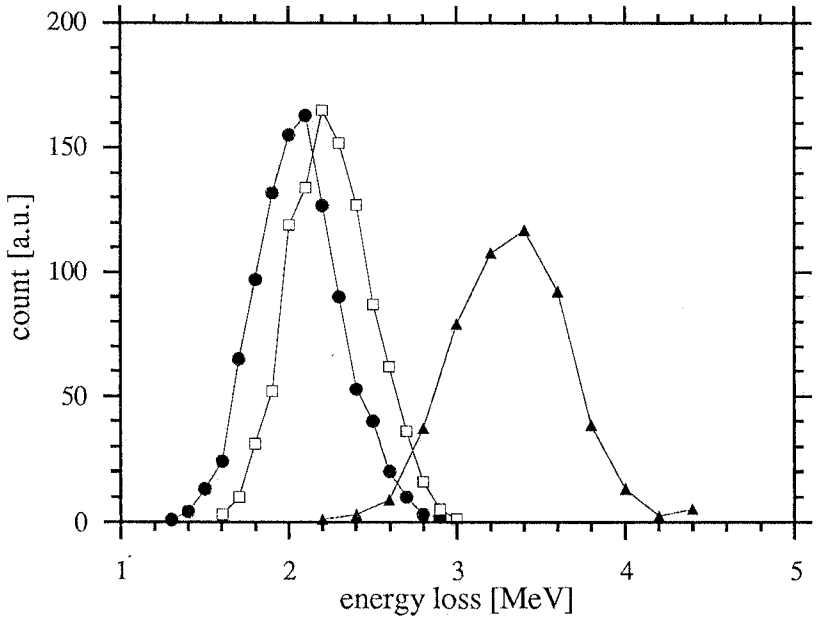

Fig. 11. *Energy loss distribution (ionization with Landau fluctuations) in the Energy Loss Detector for electrons (circles), charged pions (squares) and protons (triangles). Curves are a guide for the eye.*

c) Extended target effects. Using a cylindrical target of 1 cm radius and 2 cm length the maximum difference in path length inside the detector is 12%; so the target length must not exceed 4 cm (25% of maximum difference).

d) Angular effect. The trajectories at extreme angles (25° and 155°) will cross 2.4 cm of the scintillator against 1 cm at 90°. This factor can be corrected by the track reconstruction or by moulding the longitudinal profile of the scintillator in order to have similar

crossing lengths for each angle, if this does not affect too much the homogeneity response.

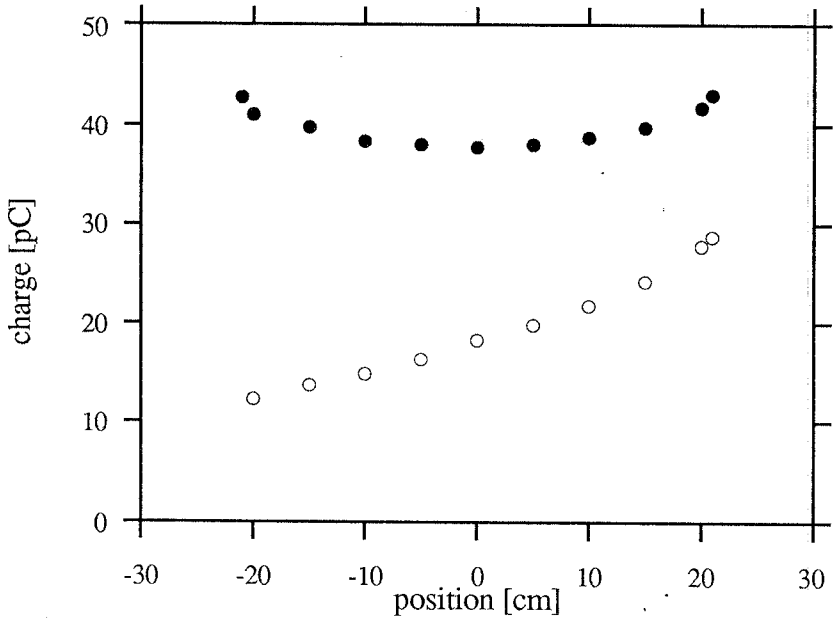

Fig. 12. *Homegeneity response of a bar of plastic scintillator viewed with one photomultiplier (open circles) or at both ends with two photomultipliers (full circles).*

2.4.2. Tracking detector.

Among the experiments proposed for the *Rugby Ball* many the request the detection of one or more charged particles. The angular resolution for charged particles (apart from showers generated by e^- or e^+) is given by the nominal aperture of the crystals ($6° \div 10°$ in ϑ, $11.25°$ in φ) if a pointlike target is assumed; this situation becomes worse when a long (4 cm) cryogenic target is considered. If the experiment requires higher precision in the determination of the emitted charged particles momenta, a tracking detector must be added to the calorimeter. The following requirements to the tracking device have been identified:

a) 1 mm spatial resolution;

b) $1° \div 2°$ angular resolution;

c) efficiency > 95%;

d) $1 \div 2$ ns time resolution;

e) maximum working rate > 10^5 s^{-1}

f) good radiation resistance.

All these requirements could be met by a scintillating fibre tracking device consisting of 2 concentric cylinders of 4 cm and 8.5 cm internal radii, respectively. On each cylindrical surface (realized in carbon fibre) there are 2 double planes of plastic scintillating fibres forming a relative angle of 60° and 30° each respect to the beam axis. Fibres can

be of the type SCIFI S101D with circular cross section and 1 mm Ø, coated with a sputtered alumination and black varnish. An Al reflector will be deposited at one end, while the other side will be used for readout. The length of each fibre does not exceed 1 m. The angular resolution is 2.5° at 90° and 0.5° in forward and backward directions; charged track vertex will be defined within 3 mm inside the target. With such a geometry the total number of fibres will be 3072: 1024 in the two internal double planes; 2048 in the two external double planes.

There are two contributions to total efficiency of each plane of fibres:

1) the probability of emitting zero photoelectrons at the photocathode, given by the Poisson distribution with a mean expectation value of 5÷10 photoelectrons;

2) the blind areas along the particle trajectory, due to cladding, coating, interstices and diameter tolerance.

Considering all these effects it is reasonable to estimate an efficiency of 95% for individual planes. If we require at least one signal for double plane on each of the 2 cylinders and in each of the 2 fibre angles, we obtain a total efficiency of 99%.

Another possibility is to use three planes on each chamber. Two planes at angles of ±30° with respect to the beam axis and the third parallel to it. If we require a signal in at least two planes in each chamber and we assume that the efficiency of each plane is 95%, then the efficiency of each chamber will be 99.3% and that of the two chamber system will be 98.6%. Very similar to the previous value of 99% obtainable with four planes.

This system has the advantage that for the 86% of the events in which all three planes fire we have a spatial resolution better by about 20% and the possibility of resolving events with two simultaneous tracks. This last characteristic is essential for the detection of events with more then one charged particle in the final state. Moreover the total number of scintillating fibres will be approximately 2300 instead of 3072. On the other side for those 10% of the events in which have fired the chamber parallel to the beam axis and only one of the other two, the spatial resolution will deteriorate by about a factor of 1.9.

The intrinsic time resolution of the fibres is equal to that of traditional plastic scintillators (<1 ns); the modal dispersion of the fibres is negligible over 1 m being less then 500 ps. So the time resolution and maximum working rate are fixed by the readout system.

Fibres with polystyrene core can work without any appreciable light yield loss up to more than 10^4 rads, depending on the dose rate and recovery times. This dose corresponds to $2 \cdot 10^{15}$ MeV of released energy in the tracking system. Considering 2.5 MeV released by a Minimum Ionizing Particle (MIP) crossing orthogonally the device, the maximum mean rate that the system can suffer over 5 years with 25% of machine run time is $2 \cdot 10^7$ s^{-1}.

For the readout of scintillating fibre detectors one can consider three different types of devices:

a) Si photodiode which however has a very high noise, greater than a factor of 10 with respect to the fibre signal.

b) Image Intensifier with a high granularity (more than 10^4 pixels per device). This system has a CCD serial readout speed of few MHz per channel and each image takes more than 1 ms to be recorded.

c) Multianode Photomultipliers (MP) which are good for systems at moderate number of channels, working at high rates and eventually participating to the process decision triggers.

The MP seem the best choice for our purpose as confirmed by tests done on a 64 channel XP4702 MP. The last dynode of this device is segmented in 64 parts, while the anode is common .

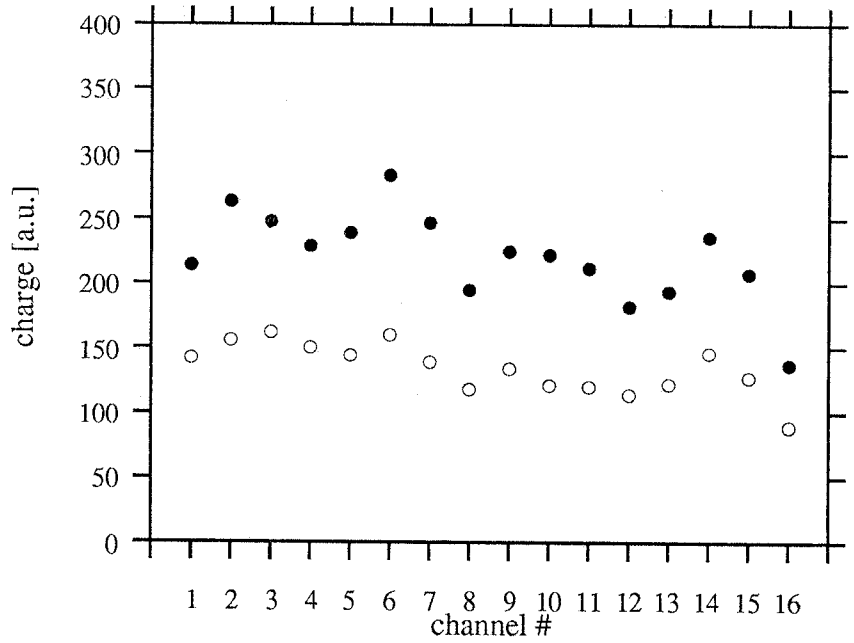

Fig. 13. *Collected charge in the 16 multianode channels at the anode (full circles) and at the dynode (open circles).*

Good results have been obtained in terms of light detection and of timing. The measured jitter is comparable to that of linearly focused photomultipliers. Some problems can arise from the crosstalk, mainly due to the light spread by the fibre end on the MP window. This effect could be however minimized using a special MP, like the XP4722, with an optical fibre glass window. Using the XP4702 as a 4x4 Photomultiplier, by coupling four channels together, the crosstalk on neighborhood channels is 5÷10%, while negligible on the others; the last dynode inhomogeneity is 30% as shown in figure 13.

Processing the signals from Multianode Photomultipliers could be realized, in a general way, in three steps:

1) amplification and discrimination;

2) registration on CAMAC;

3) acquisition.

Somewhere in the electronic chain, one has to compress the high number of channels (3072 fibres signals on 48 MP). An appropriate solution is to use a fully parallel processing system like PCOS III; this system needs for the tracking detector a total number of 192 16-Ch Amplifier/Discriminator Chamber Cards and 96 32-Ch Latching Modules. A different solution is to record on CAMAC the multiplexed serial map of the event for each MP, after a parallel amplificator/discriminator hybrid module which has to be especially designed and directly mounted on MP. Some of these modules have been developed, but nowadays they aren't commercially available.

2.4.3. Preshower detector.

The tracking system leaves a free space cylindrical crown of 4 cm thickness, that can be used as a preshower detector. This might be a BGO cylinder longitudinally segmented in 32 sectors like the energy loss detector: a 3.5 cm thickness could convert more than 90% of high energy photons. This detector might improve the angular resolution of e.m. shower because a greater number of *Rugby Ball* crystals are involved in the shower and because the external planes of the tracking system can detect the charged particles produced in the shower at that point. The only negative side is a hopefully little worsening in the energy resolution. Using the preshower detector, the anticoincidence for neutral particles is given by the internal planes of the tracking system. Finally the compared analysis of the transverse and the longitudinal shower distribution can help in the identification of charged pions from electrons, which is not possible with the energy loss detector.

2.5. Photomultiplier selection.

2.5.1. General considerations.

To select the photomultipliers for the 480 crystals of the *Rugby Ball* we have first made a choice based on catalogue figures like efficiency, effective diameter, maximum peak current, gain, maximum average current and anode rise time.

We have then acquired a few specimen of the selected types to perform some comparative tests both in response to light pulses and to radioactive sources when in combination with two prototype crystals. We were confident that even tests on a small number of tubes would have assessed the correspondence of their characteristics to the factory specifications, and eventually highlighted behaviors incompatible with their use on the *Rugby Ball*. The tests have been performed in several steps excluding from further measurements those PMT's which at some stage were found out of the required specifications. We will here recall the main results of a complete series of tests already published [9]. Bialkaly photocathodes and borosilicate windows were chosen. Only phototubes with

specified rise time below 5 ns were selected. Regarding the gain we have assumed a conversion efficiency between 50 and 150 photoelectrons / MeV [5] and imposed an anode signal not lower than 100 mV over 50Ω per E = 0.15 ÷2.00 GeV. This requires a gain G ≈ $6x10^5$.

2.5.2. Tests in combination with prototype crystals.

The sizes of our crystals impose the use of 2" or 1.5" photomultipliers. The use of specifically manufactured tubes has been discarded [9]. The choice of standard PMT's has allowed to test a reasonable variety of types and brands. Two crystal prototypes, one having the smallest and the other the largest surface coverage by the phototube window, have been tested in connection with several phototubes [8].

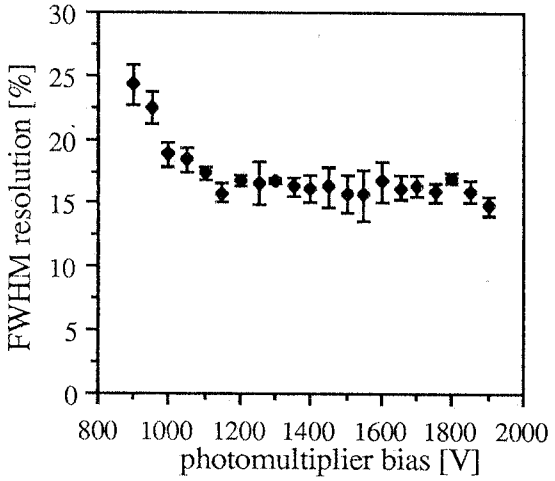

Fig. 14. *The FWHM resolution at E_γ = 661 KeV as a function of the photomultiplier bias.*

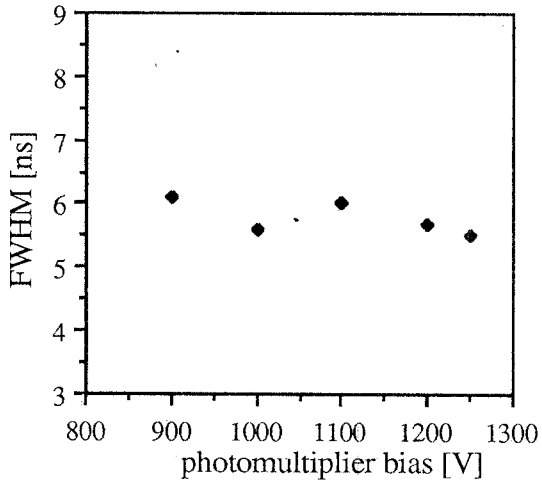

Fig. 15. *The FWHM value of the time coincidence between the BGO detector and a plastic scintillator as a function of the BGO photomultiplier bias.*

The uniformity and resolution have been measured by irradiating the crystals with a (1μC) collimated ^{137}Cs source and analyzing the anode pulses via a spectroscopy amplifier having a shaping time τ = 6 μs and a Multi-Channel-Analyzer (MCA). Four plots have been built for any PMT. The first one (figure 14) represents the resolution as a function of the PMT bias with a non-collimated Cesium source located perpendicularly to the pyramid axis of the crystal. Besides the factory typical bias value V_{typ} we determine from such a curve the minimum value V_{min} still compatible with a constant resolution. The second plot (figure 15) represents the FWHM of the time coincidence between our prototype crystals and a plastic scintillator (2x2x1 cm^3), as a function of the PMT bias. The values obtained at V_{typ} and at V_{min} are consistently higher than those reported in the

literature [10] but the discrepancy does not affect the relative validity of our measurements, as is explained by the fact that our crystals are large and compensated for longitudinal uniformity. This is achieved at the expense of total collected light. With a cobalt source the timing performance is essentially determined by the statistical fluctuation of the number of photoelectrons collected per unit time at the cathode which is strongly affected by a decrease in the total light. Assuming a dependence like $R = a/\sqrt{E}+b$ and as starting point the value R_t taken at V_{min} we have evaluated as a reference point the value E_{3ns} where the time resolution goes below 3 ns.

The third plot (figure 16) gives the energy resolution at 661 keV (^{137}Cs source) as a function of the distance from the photocathode either at V_{typ} or at V_{min}. From these curves the resolution average value $<R_E>$ from 6 to 20 cm has been extracted. Starting from the value obtained at V_{min} and assuming once again a behavior like $R = a/\sqrt{E}+b$ we have evaluated as a reference point the energy E_{1pc} at which the statistical contribution goes below 1%.

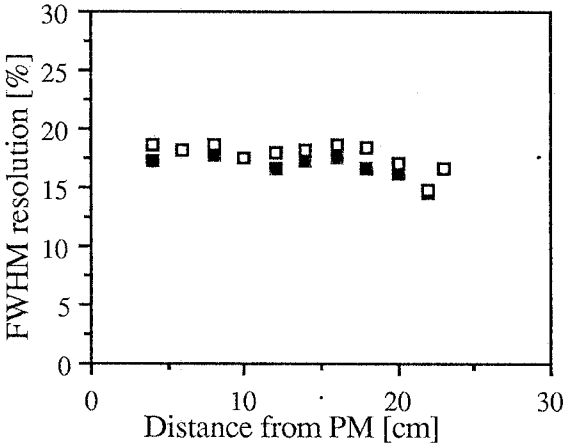

Figure 16. *The resolution at FWHM at E_γ = 661 KeV as a function of the source distance from the photocathode; full squares: V = V_{typ}, open squares: V = V_{min}.*

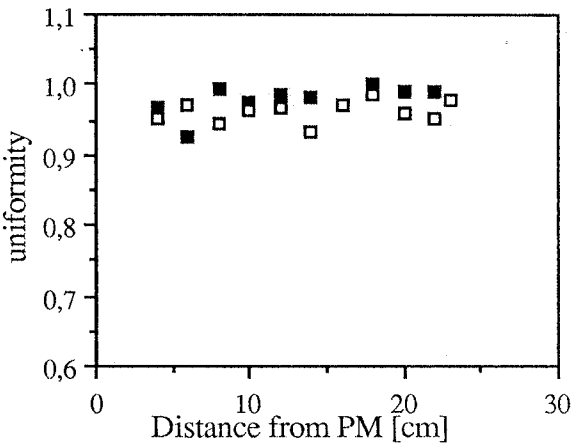

Figure 17. *The uniformity at E_γ = 661 KeV as a function of the source distance from the photocathode; full squares: V = V_{typ}, open squares: V = V_{min}.*

The plot in figure 17 represents the ratio between the peak height at some distance from the photocathode (C_x) and the maximum peak height observed along the crystal (C_M) as a function of the distance from the photocathode. The average uniformity value ($<U>$) in the range 6÷20 cm has been extracted.

Table 2 is reproduced from reference [9] and gives a summary of all quantities mentioned so far. A partial factor of merit, normalized to 100, has been defined as

$$F_{BGO} = \frac{<U>^2}{E_{3ns}\, E_{1pc}}$$

The second power of the uniformity has been taken considering that all values are close to

1 and to each other. Partial results could already exclude those specimen that did not achieve a factor of merit of 50. It should be remarked that the uniformity is very similar from tube to tube stressing the fact that it depends uniquely on the treatment of the BGO surface; therefore our attention focused on other PMT's features.

TYPE	V_{typ} [V]	V_{min} [V]	$<R_E>$ at V_{typ} [%]	$<Ris_E>$ at V_{min} [%]	E_{1pc} [MeV]	<Unif> at V_{min}	$<R_t>$at V_{min} [ns]	E_{3ns} [MeV]	F_{BGO}
R329	1500	1200	17.3	17.9	210	0.964	4.6	3.5	92.7
R1306	1000	600	16.2	16.2	174	0.974	9.4	16.7	23.8
R1847	1000	700	17.6	18.5	227	0.966	6.0	6.3	47.2
R2154	1250	850	18.0	18.3	222	0.976	7.2	9.4	33.3
9256	1000	750	15.9	16.5	180	0.965	4.8	3.8	100
9257	1000	750	14.6	15.9	16.7	0.974	6.0	6.3	72.5
XP2202	1150	800	18.8	19.7	257	0.980	7.0	8.9	30.8
R580(*)	1600	900	21.9	22.3	329	0.983	5.2	4.6	47.0
R980(*)	1000	650	19.3	19.7	257	0.981	5.3	4.8	57.6

Table 2. *Test results with prototype BGO crystals. (*) indicate 1.5" phototubes*

2.5.3. Tube tests.

A further series of tests has concerned: linearity, maximum peak current, temperature stability, gain variation with average current, linearity in terms of energy, measured at V_{typ}, V_{min} or both. The apparatus [11] consists of a light tight tube where three LED's (HP1540 green) shade light pulses on the photocathode. Different pulses on LED's give anode charges A, B...which are read at channels C_A, C_B.... When LED's are pulsed in coincidence, the corresponding total charge Q must be read at $Ch = C_A + C_B + \ldots$ Deviations from this relation can be identified in plots like that in figure 18.

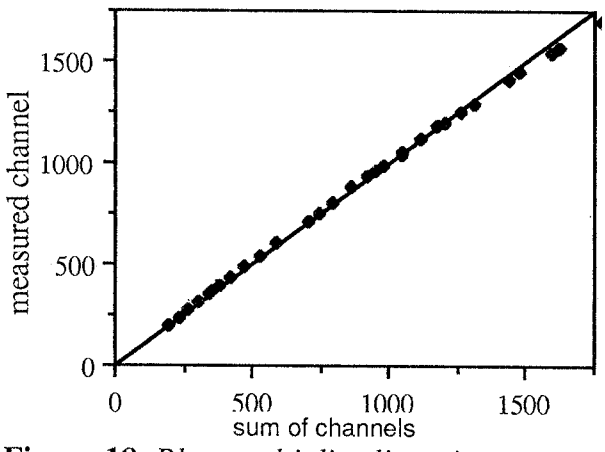

Figure 18. *Photomultiplier linearity.*

When the points deviate approximately 2% from a straight line the anode pulse is read by a digital scope at 150 MHz and the total charge in the pulse, the peak current and the average current are taken. Keeping the LED's in the very same situation, the pulses repetition rate is increased until a further 2% deviation in the peak value is observed. This gives a measure of the maximum

tolerable peak current at the limit of linearity. For tubes showing complex results such as large fluctuations around the straight line, or departures from linearity already at low peak currents, no other tests were made. For the rest of the tubes the linearity test was repeated with pairs of exponential pulses as described above. The peak current found in this case was consistent with that obtained with square pulses.

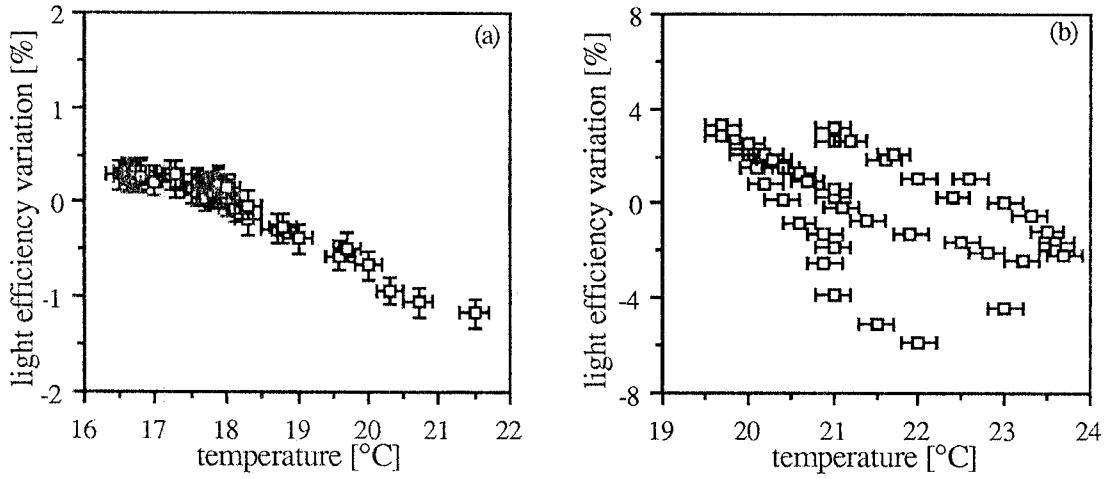

Fig. 19. *The temperature behaviour over a long time period of some photomultipliers: (a): stable PMT, (b): a case of hysteresis.*

An approximate estimate of the energy corresponding to maximum linear conditions has been made comparing the LED output to a pulse generated by a so called *Light Pulser*. This consists of an Americium alpha source dispersed over a little NaI scintillator. LED pulses correspond to an energy value E_{sat} computed knowing that the γ equivalent energy of americium is 2.4÷3.6 MeV and that the efficiency ratio BGO/NaI is 0.10÷0.12. For those tubes which had an E_{sat} value at V_{min} below the application range of the *Rugby Ball* no further tests were performed.

The *Light Pulser* has been used to check the temperature related gain variations over long time periods. The curves that are produced (figure 19) reflect basically the variations of light efficiency of the NaI, which has a temperature coefficient of 0.22%/°C [6]. Some of the tubes show a percent gain variation that is basically corresponding to the $\Delta G/\Delta T$ known for NaI. The behavior is linear with high regression coefficients (figure 19a). This proves a good stability in time. Some other do show hysteresis (figure 19b) and must be discarded. The fitted angular coefficient is as better as it approaches the NaI value. The regression coefficient can be taken as an indicator of good time stability. This second set of parameters is reported in Table 3 including A_{150}, i.e. the anode pulse height extrapolated at 150 MeV.

TYPE	I_p^{sq}[mA]	$\langle I_A^{max} \rangle$ [μA]	I_p^{exp} [mA]	E_{sat}[GeV]	ΔG/ΔT [%/°C]	C_{reg}^T
R329	103.6	18.0	112.0	0.6÷1.2	0.32	0.96
R1306	17.4					
R1847	30.0	34.0	33.0	1.0÷1.9	0.44	0.90
R2154	50.0	25.0	56.0	0.3÷0.6	0.30	0.95
9257	48.0	12.6				
9939	152.0	19.5	94.0	0.2÷0.3	0.36	0.60
2212	> 284.0	53.0	340.0	0.1÷0.2	1.06	0.56
R580(*)	100.0	8.0	106.0	8.4÷15.1	0.46	0.92
R980(*)	17.0	3.8	17.2	0.6÷1.2	0.56	0.72

TYPE	I_p^{sq}[mA]	$\langle I_A^{max} \rangle$ [μA]	I_p^{exp} [mA]	E_{sat}[GeV]	A_{150}[mV]	F_{mer}
R329	47.0	15.2	43.0	1.4 - 2.4	190	13.0
R1306	5.7	6.7				
R1847	13.6	7.6	13.6	1.3 - 2.4	60	2.1
R2154	24.0	9.5	28.0	3.7 - 6.7	34	
9256			31.0	0.1 - 0.2	17	
9257	32.0	9.2		0.1 - 0.2		
9939	70.0	5.8	26.0	0.4 - 0.6	390	
2212	> 60.0	47.0	82.0	0.5 - 0.9	880	
R580(*)	35.0	4.3	36.0	9.7 - 17.4	16	7.6
R980(*)	3.5	1.8	3.4	2.7 - 4.9	7	0.4

Table 3. *Test results with prototype BGO crystals. (*) indicate 1.5" phototubes*

2.5.4. Analysis of results.

The final choice has been made combining the results of Tables 2 and 3. Tests in combination with prototype crystals would have already excluded a few PMT's. Nevertheless we have thought it reasonable to extend the testing for those tubes which stood out because of compactness and low cost. A primary selection rule has been the energy range at which the *Rugby Ball* should operate (150-2000 MeV). Linear responses up to 1 GeV are recommended. Then we have considered the timing performances of our phototubes. We have extrapolated the 1.17÷1.33 MeV results to higher energies. Those tubes which have time resolutions above 6 ns at the energy of a cobalt source must be discarded. For the remaining tubes a factor of merit has been calculated to weight appropriately all the measured parameters.

$$F_{mer} = \frac{E_{sat}\ A_{150} C_{reg}^{T}}{R_t\ \langle R \rangle_E\ \Delta G/\Delta T}\ .$$

The factor of merit will be higher for the best tubes. From the reported values it appears quite clearly that the Hamamatsu R329 (2") and the Hamamatsu R580 (1.5") are those that gave, in our tests, the best performance. On these tubes some double checks have been made, repeating the tests on different samples of the same tube with basically similar results [11]. In the case of the R329 tube, which performs linearly in an energy range just within the required limit, we have decided to order linearity selected PMT's. In this case a further series of tests has been performed on several selected tubes to establish a correlation between the linearity results obtained by our method and the values measured during the factory production with a different method. To exclude possible systematic differences a reference tube has been selected to which all the others will be matched.

3. THE RUGBY BALL FIRST LEVEL TRIGGER

3.1. Background evaluation.

The first trigger logic design requires beforehand the evaluation of the expected event rate at the electronic front-end. The logic will then select the true events out of the background mainly due to electromagnetic interactions.

The background has been evaluated using a Montecarlo simulation of an intense ($R_{tagging} = 10^7\ s^{-1}$ in the photon energy range 600÷1200 MeV) photon beam on a 1 cm thick ^{12}C target. To the *Rugby Ball* counting rate contribute: i) the nuclear reactions products that are in coincidence with one tagging channel, ii) the electromagnetic reactions products that are in coincidence with one tagging channel, iii) the nuclear reactions products that are in random coincidence with one tagging channel and iv) the electromagnetic reactions products that are in random coincidence with one tagging channel.

i) Only the nuclear contribution has a physical interest while the others produce a background that the first level trigger logic must suppress. We examined these contributions more in detail by considering first the effect of the discrimination of the signal of a single crystal (*trigger a*) and then the effect of the discrimination of the total energy detected by the *Rugby Ball* (*trigger b*). In this study a threshold corresponding to 3 MeV for the (*trigger a*) and to 10 % of the tagged photon energy for the (*trigger b*) is used. The meaning of (*trigger a*) will become clearer with the discussion of the acquisition system for the linear signals.

ii) In figure 20 (a) the expected rate in the *Rugby Ball* solid angle is reported as a function of the polar detection angle ϑ. Each point corresponds to the expected counting

rate of the 32 BGO crystals placed at the same ϑ angle and the different symbols correspond to different discrimination thresholds

The background contribution, corresponding to $R_{BGO} = 10^3$ s^{-1} on the whole detector, is reduced to 10^2 s^{-1} after *trigger a* and further reduced to $R_{ii} = 1$ s^{-1} after *trigger b*.

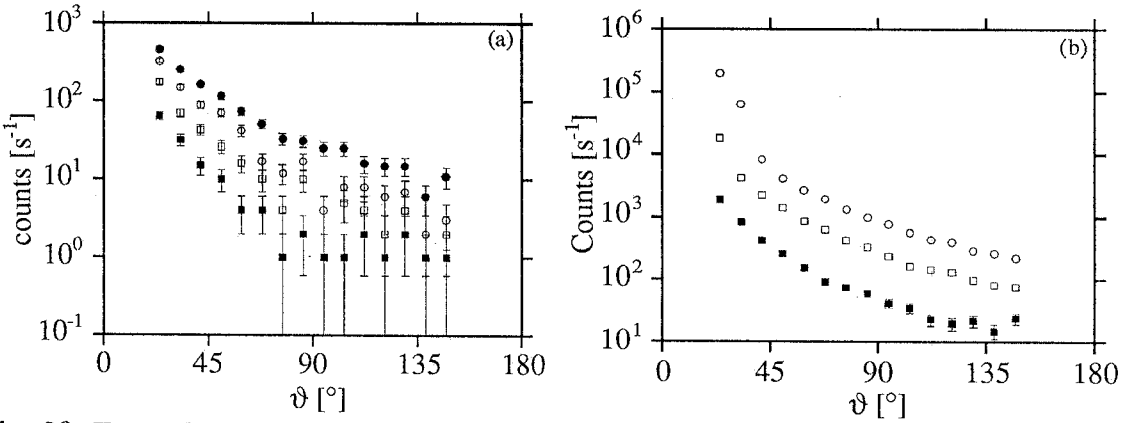

Fig. 20. *Tagged (a) and total (b) electromagnetic background produced by an intense (10^7 s^{-1}) tagged photon beam impinging on a thick (1cm) ^{12}C target as a function of the polar angle ϑ and integrated over the azimuthal angle φ. Full circles: total contribution; open circles: contribution above 1 MeV; open squares: contribution above 3 MeV; full squares: contribution above 10 MeV.*

iii) This contribution, equal to $R_{BGO} = 10^4$ s^{-1}, arises mainly from the interaction in the Δ region that is below the tagging energy range. In this study, it has not been possible to evaluate the effect of *trigger a* and *trigger b* , however the evaluation of the random coincidence, in the hypothesis of a $\tau_{coin} = 10$ ns coincidence with the tagging hodoscope, gives a random coincidence rate $R_{iii} = 2\ 10^3$ s^{-1} derived from the expression

$$R_{iii} = 2\, R_{BGO}\, R_{tagging}\, \tau_{coin} = 2 \cdot 10^4 \cdot 10^7 \cdot 10^{-8} = 2 \cdot 10^3 \text{ s}^{-1}.$$

With an accelerator operating at a frequency f = 300 Mc and an electronics which can resolve events produced in two distinct RF pulses, the fraction ϕ of RF pulses occupied by tagging events is:

$$\phi = R_{tagging} / f = 10^7 / 3 \cdot 10^8 = 1/30$$

and the random coincidence rate, R'_{iii} , will be:

$$R'_{iii} = 10^4/30 = 3.3 \cdot 10^2 \text{ s}^{-1}$$

iv) This is the main contribution and it arises from the random coincidence of the tagging hodoscope with the pair production from low energy photons. In figure 20 (b) the expected rate in the *Rugby Ball* solid angle is reported as a function of the polar detection angle ϑ.

The background contribution, corresponding to $R_{BGO} = 10^6$ s^{-1} on the whole detector, is dominant at angles less than 80° and reaches the value of 10^4 s^{-1}/crystal on the

forward crystals. *Trigger a* reduces the background rate down to 10^3 s^{-1} that produce a random coincidence rate $R_{iv} = 10^3$ s^{-1}. *Trigger b* further reduces the counting rate down to $R_{iv} = 40$ s^{-1}.

The contribution of the cosmic background to the random coincidence rate has been evaluated considering a uniform cosmic ray flux of 2.10^{-2} cm^{-2} s^{-1} upon the sphere. This corresponds to a rate of 1 s^{-1} that produces the random coincidence rate $R_{cb} = 0.25$ s^{-1}. So far, the effect of *trigger b* has not been evaluated.

coincidence type	source	total [s^{-1}]	after trigger a [s^{-1}]	with tagging coincidence [s^{-1}]	after trigger b [s^{-1}]
true	e.m	$1.3\ 10^3$	$0.14\ 10^3$		1
	nuclear	$2.5\ 10^3$			
random	e.m.	$0.86\ 10^6$	$3.9\ 10^3$	$0.78\ 10^3$	40
	nuclear	$30\ 10^3$		$6\ 10^3$	
	cosmic	$0.12\ 10^3$		24	

Table 4. *Expected acquisition rate for the different processes with and without triggers.*

The previous counting rate has to be compared with the true event rate $R_i = 2.5\ 10^3$ s^{-1}. The results are summarized in table 4 where the effect of each trigger has been pointed out. It is clear that the electromagnetic and cosmic ray backgrounds are three orders of magnitude lower than R_i , R_{iii} is still comparable with R_i and a more detailed evaluation of *trigger b* effect must be performed.

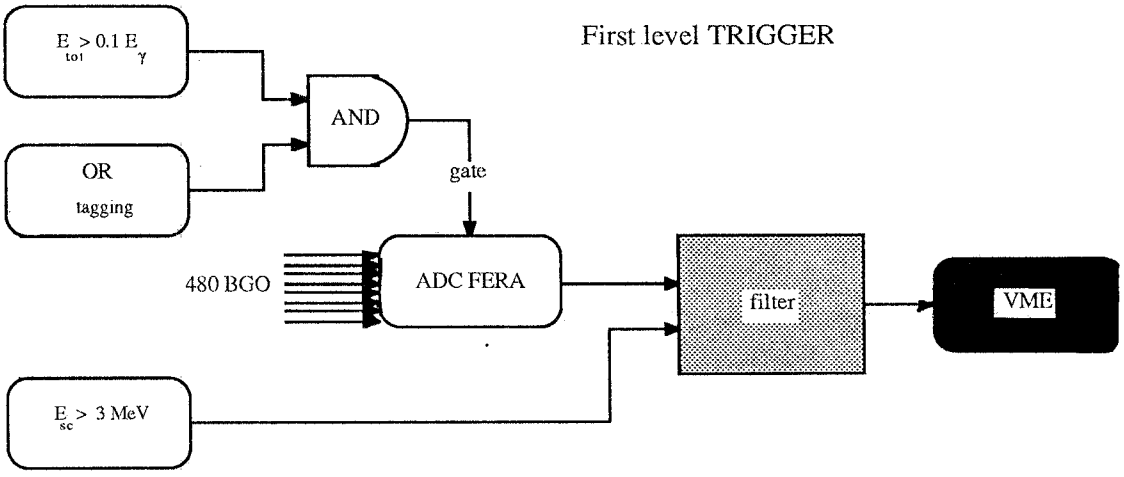

Fig. 21. *First level trigger.*

Furthermore, the AND coincidence between *trigger a* or *trigger b* and the tagging signal provides the gate for the linear acquisition. *Trigger a* acts also as pile-up rejection device: the pile-up rate of a single crystal (defined as the pile-up of a true signal with a noise higher than 3 MeV), in the 100 ns ADC integration time, is equal to 1 s^{-1}. In spite of this the noise arising from different crystals is 500 times higher. This rate can be reduced, after the ADC conversion, realizing a digital filter that compares the ADC converted values with the almost instantaneous 3 MeV map of the crystals. In this case the total pile-up rate would be 2 s^{-1}. In figure 21 the first level trigger logic is reported.

3.2. Linear acquisition.

A major problem is the data-transfer rate: the conversion and transmission of data correspond to a dead time that must be reduced as much as possible. The linear acquisition system is based on the ADC FERA system composed by a certain amount of ADC FERA converters (internal threshold of which will be fixed to the 3 MeV value), one ADC FERA Driver and one or more Data Stacks or Memories. We studied the effect of the division of the FERA acquisition line into different ECL lines (and consequently different FERA Drivers and Data Stacks) serving the same number of baskets. An ADC FERA takes less than 8 μs to convert the input signals. After that time the device is ready to transmit the converted values on the ECL bus towards the Stacks at a transmission speed of 130 ns/data with a 270 ns commutation time. All the data, starting from a parallel configuration (all ADC convert simultaneously), must converge in a sequential flow. In table 5 the effect of a gradual reduction from parallel to sequential flow is reported. The conversion and transmission time is evaluated as a function of the number of ECL lines in the hypothesis of a first level trigger rate R_{flt} equal to 10^4 s^{-1} (columns t+r obtained without the rejection of the nuclear background R_{iii} and 2.5 10^3 s^{-1} (columns t obtained with the rejection of the background).

The values have been obtained from the equation

$$\tau = 8 + 0.13n_d + 0.27n_{ADC} \quad [\mu s]$$

where n_d is the number of converted detectors and n_{ADC} the number of modules. The minimum values were obtained in the hypothesis of only one detector signal and the maximum in the hypothesis of 120 detector signals. The probability that a second signal arrives at the logic set-up during the conversion and transmission procedure is also reported; it was evaluated by the expression

$$p = 1 - \exp(-R_{flt}\,\tau).$$

The effect of nuclear background rejection is non negligible and must be evaluated more in detail. However it seems that an ECL line number higher than four could guarantee a reasonable dead time; on the other side the higher the ECL line number is, the more expensive the system is. Thus all the following evaluations were performed with the minimal configuration of four ECL lines.

ECL lines	τ_{min} (μs)	τ_{max} (μs)	p_{min} (t+r)	p_{max} (t+r)	p_{min} (t)	p_{max} (t)
1	16.50	31.97	.15	.27	.04	.08
2	12.18	27.65	.11	.24	.03	.07
3	10.83	26.30	.10	.23	.03	.06
4	10.02	25.49	.10	.23	.02	.06
6	9.35	19.75	.09	.18	.02	.05
8	9.01	16.81	.09	.15	.02	.04
12	8.68	13.88	.08	.13	.02	.03
24	8.34	10.94	.08	.10	.02	.03

Table 5. *Minimum and maximum transfer time of the FERA system, Minimum and maximum dead time as a function of the number of ECL lines (t) true coincidences, (r) random coincidences.*

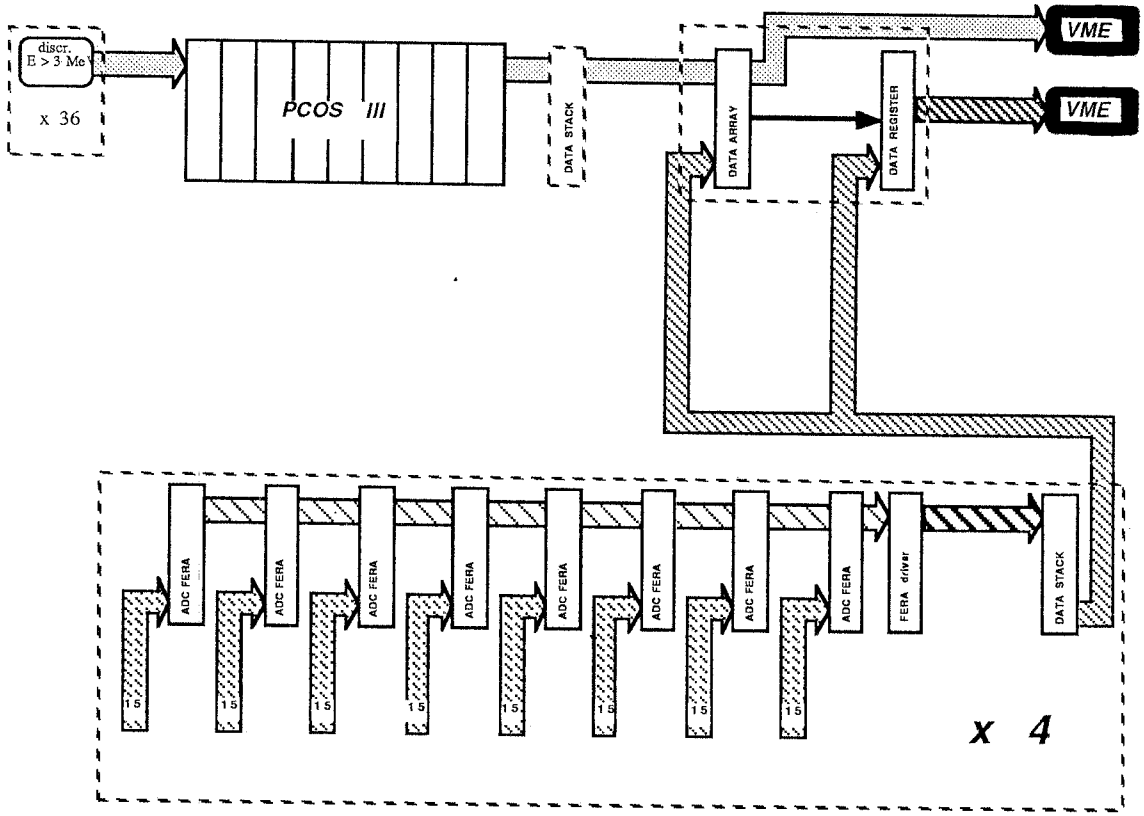

Fig. 22. *The data acquisition scheme with filtering.*

Before the second level processing, the data, as mentioned before, has to be filtered. The instantaneous 3 MeV map can be realized using a LeCroy PCOS III-like device. The map is built and stored in a Data Array during the ADC conversion and transmission time. The Data Array will be then asked by the single linear data. PCOS III takes 100 ns to read 32 discriminators and, while it is reading, an encoder processes the previous data

generating the addresses of detectors at 10^7 s^{-1} In a bad condition, when half of the 480 detectors generate a signal, the storing procedure takes 24 μs, less than the conversion and transmission time of the linear acquisition system.

In figure 22 the whole filter device is shown: the PCOS III signals enter both in a data array and in a VME crate for the second level trigger processing, while the ADC converted signals, after being stored in a Data Stack, enter into the VME crate through a Data Register that is open only if the Data Array gives a positive answer.

4. CALIBRATION AND MONITORING

4.1. General considerations.

At any stage of the life of an electromagnetic calorimeter (EMC), one needs to know the correspondence between the charge Q collected and converted by the data processing, and the effective energy E released in the EMC. In other words the error induced by the uncertainty in the absolute energy scale is added to the statistical uncertainty. In time, it is difficult to control this systematic error because of uncorrelated effects like material ageing, radiation damage, temperature variations, PMT's bias instabilities. The necessity of limiting and controlling these effects is clear because the energy scale must be known with more precision than the energy resolution of the apparatus. Two complementary approaches can be normally used: calibration and monitoring.

Calibration consists in establishing the relation $Q = cE$ with physical events of known energy. Monitoring consists in probing and correcting any energy scale derivative $c = c(t)$ with reference to known light or charge quantities. The calibration fixes an absolute energy scale using the same procedure that will be adopted to treat physical data of interest. Anything between the detector and the data sorting is controlled in one goal. This can be performed once in the lifetime of the EMC in parallel with monitoring by some known and reproducible light pulse. This light pulse will then monitor variations over long periods of time. The calibration of an EMC, which does operate in a large energy range, obviously requires the determination of a linearity curve including several points and therefore requires a complex apparatus to work with a variable energy beam. It is a technical effort that we are planning to do at Frascati at the JET-TARGET tagged photon beam and that will take advantage of the modularity of our *Rugby Ball.* Individual baskets will provide ideal support to irradiate reasonably large clusters of crystals with suitable beams.

4.2. The monitoring technique.

Monitoring requires that the quantity of light injected in any crystal is stable in years to an accuracy better than the EMC energy resolution. The gain variations δG of PMT or

electronics can be spotted and corrected by changing the PMT high voltage. Three are the main components of a monitoring set-up: the light source, the distribution system and the synchronization and normalization.

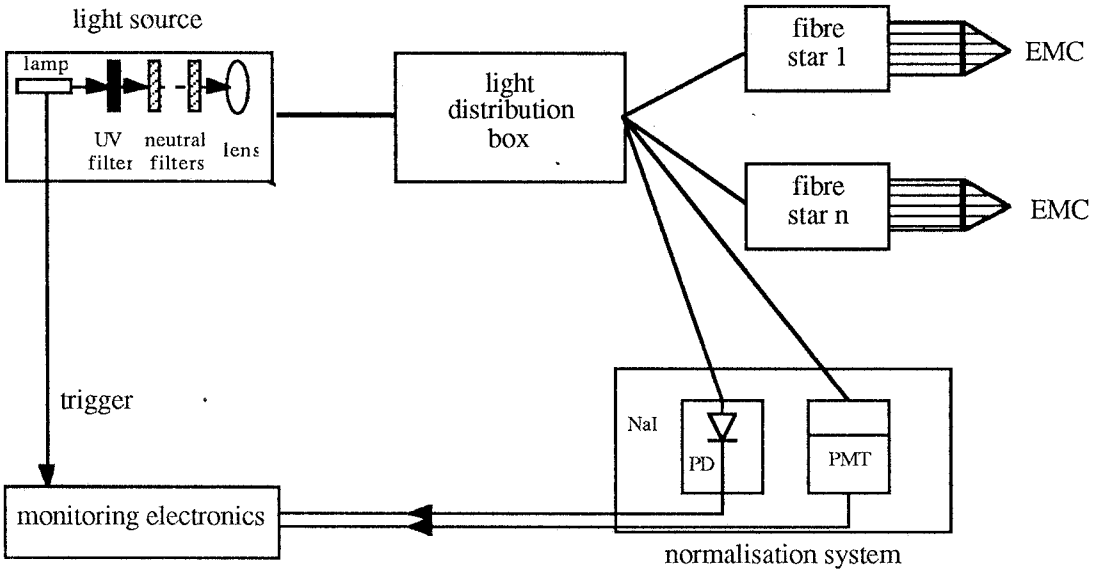

Fig. 23. *General layout of the monitoring apparatus.*

The source should have a stability better than 1% and in any case its output must be controllable to such a precision. The emission spectrum must match the spectral response of the bialkaly photocathodes and the source must respond to pulses, having rise and decay times comparable to those generated by a scintillation event. The distribution and normalization system does not depend on the type of light source chosen. We are presently considering to test the distribution system with a Xenon lamp marketed by Xenon Corp. (mod. N789B-1+437A) having a peak power P_p = 50 kW. The number of photons emitted in the window 400/600 nm is $N_{ph} = 1.5 \cdot 10^{17}$ [ph/200 nm/J in]. The BGO light emission is of the order of $N_{ph}^{BGO} \approx 10^4$ ph/MeV which makes a total of $5 \cdot 10^6$ photons at 1.5 GeV. The problems connected with the use of such a source are the relatively low lifetime and an appreciable UV emission which must be filtered because it can damage the BGO crystals. Meanwhile we are exploring the possibility of future system configurations incorporating a dye laser as the light source. We are presently testing a basic scheme of monitoring depicted in figure 23. UV filtering will be specifically investigated regarding the effect of UV light on filter heat centers which may on a long time base appreciably modify the transmitted spectrum.

If the light source is a dye laser a UV filter will not be required. In fact it will be possible to tune the wavelength of the light emission in order to eliminate the UV component. As for the intensity tuning we are testing neutral high precision (±1%) quartz filters in various combinations.

The most complex part of the system is the light diffuser. Different solutions are reported in literature [12,13,14] their aim is to produce a light output as uniform as possible on all exit channels. Emi-spherical, cylindrical or conical shapes have been produced. We shall thoroughly experiment on a cylindrical diffuser where output fibres depart from the curved surface. The appropriate material for such fibres is polystirene, which is known to better stand high radiation doses. Each main fibre will be splitted by a commercially available mixer, providing also an intensity regulation. Two or three main fibres will connect the diffuser to the normalization and synchronization electronics.

4.3. Normalization.

Specific attention has to be paid to the normalization of the light pulses. As a matter of fact it looks quite reasonable to accept sources that are intrinsically less stable (3%) than others and monitor them, instead of paying a high price for a very stable source which should be after all equally normalized. Some of the systems actually adopted can be discussed. The L3 detector at LEP[14] uses two independent devices : a PMT and a PD which both read the light source. In addition the PMT reads the light produced on a thermostated NaI scintillator by a Cs source. The three readings provide double checks on the stability of the light source and of the PD itself. Over a period of a few days an excellent performance of the PD is generally found. The synchronism is given by a reference trigger of the light pulse generator.

In ARGUS [13] these two independent systems are again a PD and a lead glass read by a PMT. Here the reference energy is not the Cs peak but the energy deposited in the lead glass by muons whose trajectory is identified by a four-fold coincidence. The limit of this system is in the low muon count rate (1.8 muons/s^{-1}) which implies long measure times (80 min) if a one percent statistical accuracy is required. The reliability of the PD's and the versatility of the L3-like system will be experimented first.

5. MONTECARLO SIMULATION OF THE RUGBY BALL

The electromagnetic shower code GEANT3 [15] was used to simulate events in the calorimeter in order to obtain response functions for energy deposition, angular resolution and mass identification of neutral particles. A full geometrical description of the detector was used including all crystals (TRAP shape of the GEANT3 geometry package) and the carbon fibre support structure. A 2 cm long 4 cm diameter mylar cylinder containing liquid hydrogen was used as a target for event simulation. A gaussian beam with a radial distribution with σ = 0.6 cm, corresponding to the shape of the JETTARGET beam, was used. As a first step, and in order to have the cleanest

information about the possibilities offered by the calorimeter, no central equipment was included in the simulation.

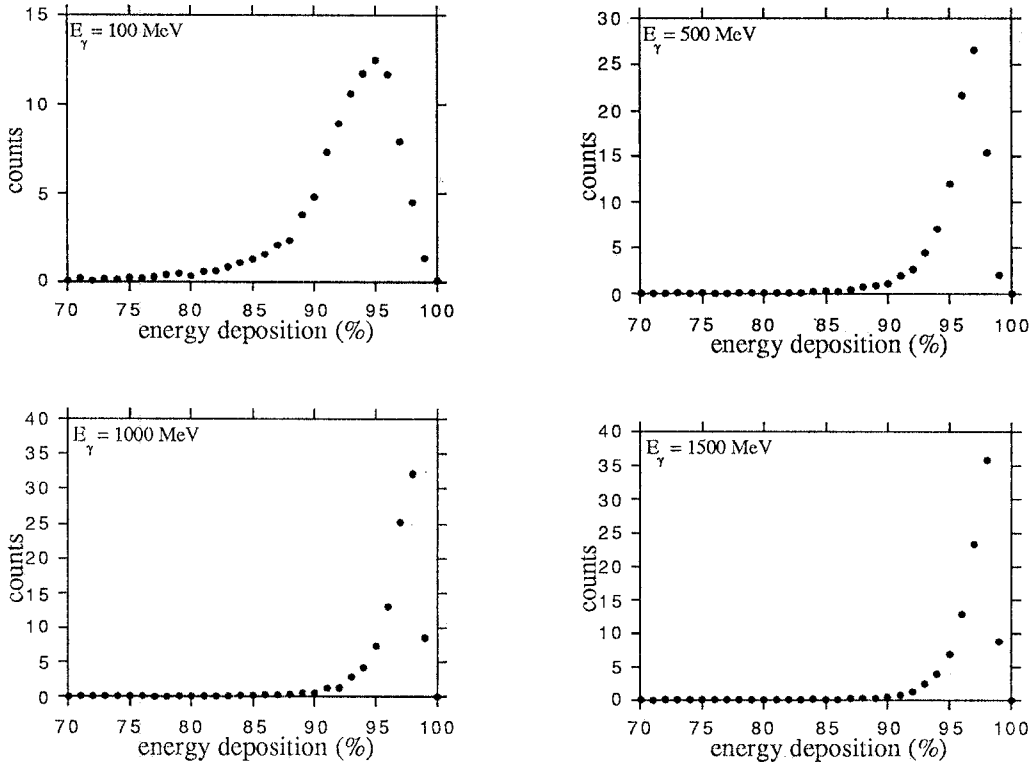

Fig. 24. *The Montecarlo response functions at the given photon energies.Counts are in arbitrary units.*

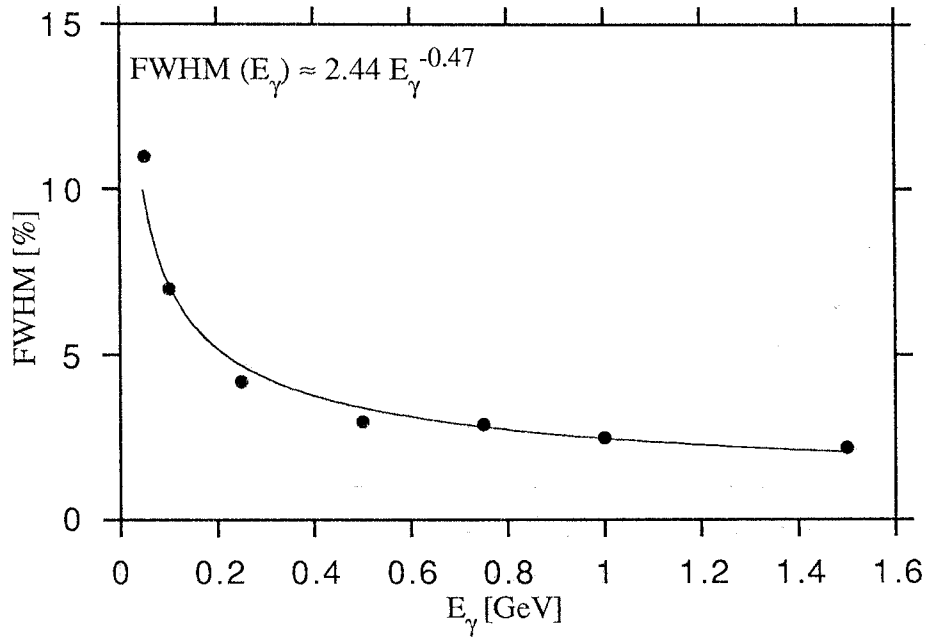

Fig. 25. FWHM energy *resolution at FWHM as a function of the incoming photon energy.*

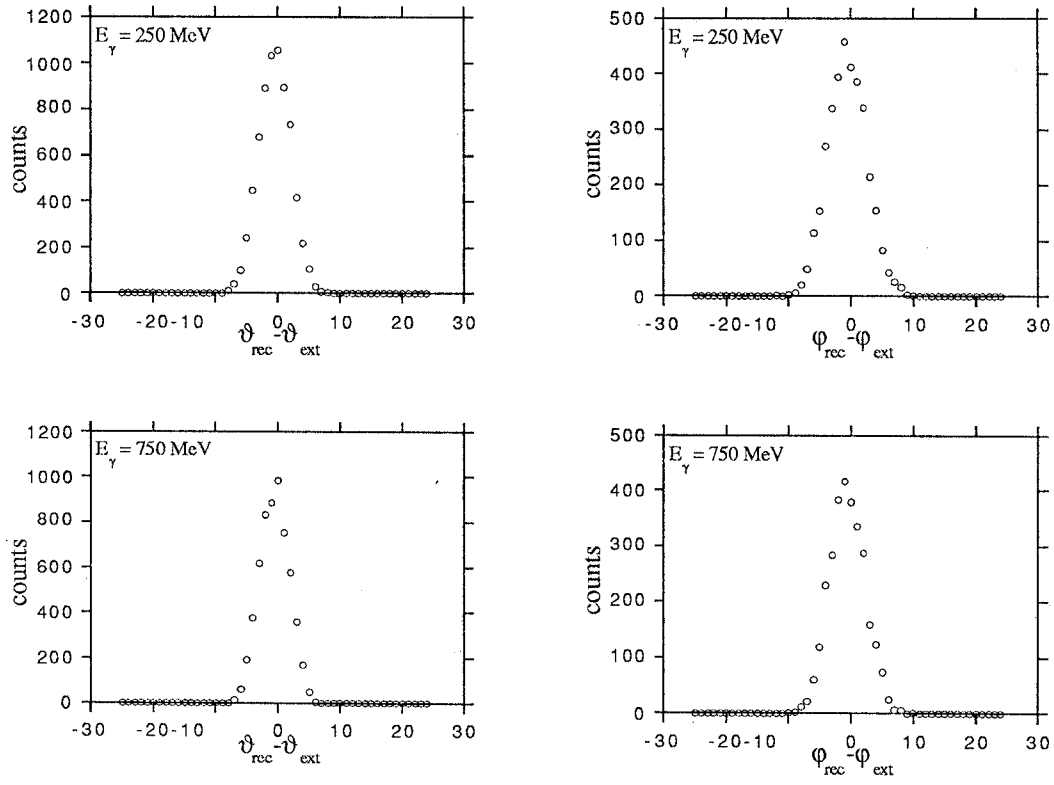

Fig. 26. *Response functions at the given photon energies for ϑ and φ baricentral reconstruction.Counts are in arbitrary units, abscissa are in degrees.*

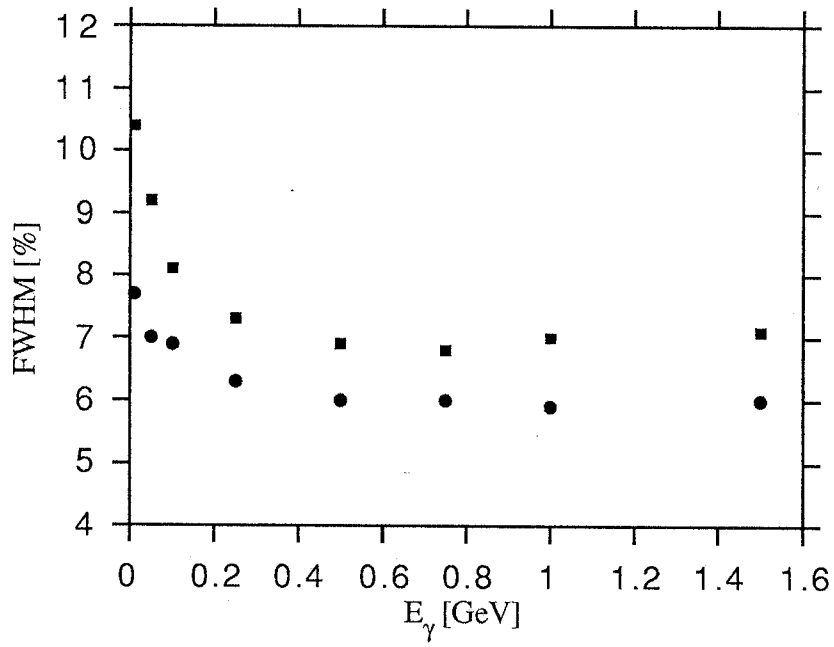

Fig. 27. *FWHM angular resolution for ϑ (circles) and φ (squares) baricentral reconstruction as a function of the incoming photon energy.*

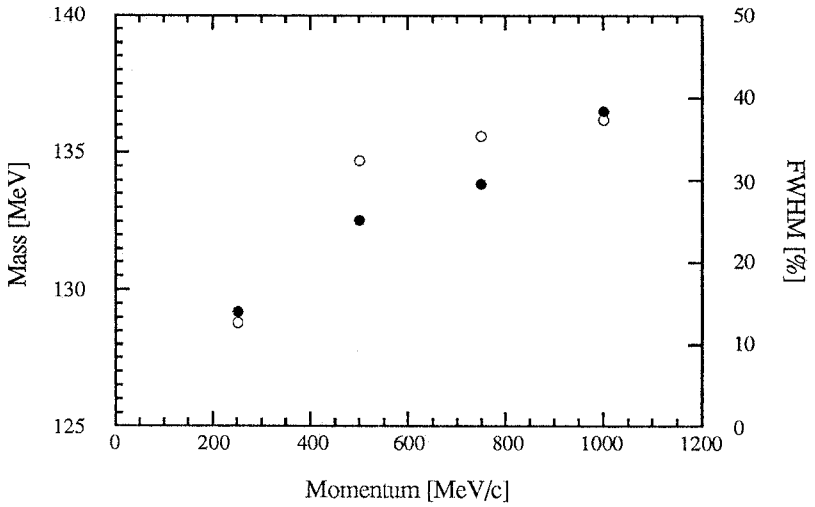

Fig. 28. *Centroid (open circles) and resolution at FWHM (full circles) for neutral pion mass reconstruction as a function of pion momentum.*

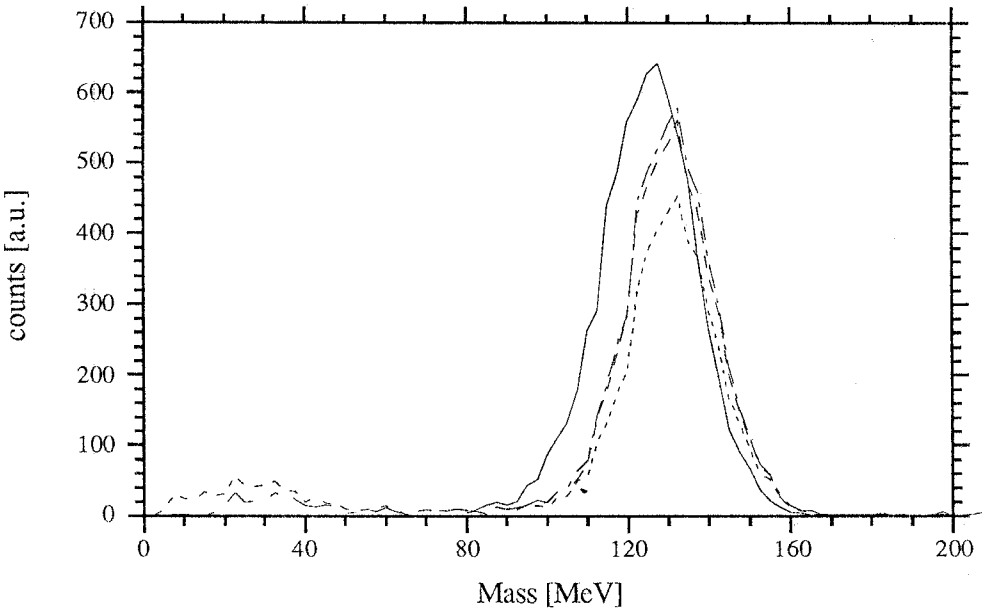

Fig. 29. *Response functions to neutral pion mass reconstruction with different reconstruction techniques (see text).*

In figure 24 some of the response functions of the detector at the given photon energies are shown. A 3 MeV threshold will be used in the discriminators and is included in the simulation. The length of the crystals and the very thin, low Z, inert mechanical support, allow a quite complete containment of e.m. showers giving rise, for the resolution as a function of the incoming photon energy (figure 25), to a behavior very close to $E^{-0.5}$.

Angular response functions for photons are shown in figure 26 for ϑ and φ reconstruction. The angular resolution displays, for both angles, a constant behavior as a function of the energy for $E_\gamma \geq 200$ MeV indicating that photon showers have a topology independent of the incoming energy (figure 27). It is noticeable that, despite the large granularity of our detector, barycentric angle reconstruction allows to obtain resolutions that are 40% smaller than the nominal angular aperture of our crystals. Target effects, crystal volume effects and different centroid angle reconstruction, were studied for photon showers. Results indicate that the relevant quantity for a barycentral determination of the photon angle is the energy deposition per unit volume and that targets longer than $\approx$ 3 cm can be used only if a central preshower and tracking detector is added to the *Rugby Ball.*

The angular and energy resolution of electromagnetic showers have direct effects on the reconstruction of neutral particle masses. The effects have been studied directly by simulating in the sphere the detection of neutral pions of variable momentum. In particular we have studied the effect on the mass resolution and on the detection efficiency of different reconstruction techniques, both to establish the limits of the system and to identify the most suitable algorithms to be implemented in the data analysis programs. A trivial technique identifies the two maxima in the 480 bins map of energy deposition; then theinformation contained in the eight adjacent crystals is considered to obtain the energy and the angle of the two showers. The centroid and FWHM resolution, of the mass distributions obtained with this method as a function of π^0 momentum are given in figure 28. Several other attempts have been made. Two 480 bins maps have been assumed, one relative to the sectors which detect more than 3 MeV, the other relative to a higher threshold corresponding to 2% of the pion energy. The 3 MeV map is in principle more complete but entails, specially at the higher momenta, the possibility that two merging showers are not identified and that small energy spills (due to the large mean free path of low energy photons) are mistaken as individual showers. Correction of these effects is possible but at the expenses of detection efficiency. The high threshold map carries a reduced energy information, but the identification of cluster pairs is very close to the efficiency limit allowed by the 78% of the total solid angle covered by the *Rugby Ball* . The systematic error in the mass distribution centroid and the larger FWHM may well be tolerated due to large difference between the π^0 and η masses. Some results obtained by the different techniques are shown in figure 29.

6. CONCLUSIONS

The activity of the BGO collaboration has obtained up to now some fundamental results:

a) The geometry of the crystal ball has been fully defined and a reasonable compromise has been found between apparently conflicting requirements:

i) a good energy resolution ($\approx$ 2 % FWHM) at a gamma ray energies up to 1.5 GeV with an acceptable cost and size (a thickness of 24 cm or 21 r.l.);

ii) a sensible angular resolution to photons ($\Delta\vartheta \approx 6°$, $\Delta\varphi = \approx 7°$ at FWHM for gamma ray energies greater than 200 MeV) with a reasonable number of crystals (480) and the introduction of a very small amount of non-scintillating material inside the ball;

iii) an inner bore of 10 cm radius which will allow the use of cryogenic targets and a vertex detector to measure the angle of charged particles with a precision of $\pm 1°$ and their point of origin with a precision of $\pm$ 2 mm.

b) Prototype crystals of different sizes have been tested and found to have the required properties of uniformity and energy resolution. A computerized testing device has been built and already used for the test of the first 80 crystals;

c) To hold the crystals in position, with a minimum of inert material between them, a carbon fiber structure consisting of 24 crates has been designed and built. Each crate contains 20 crystals. The maximum thickness of the walls is (0.54 x 2) mm. In this way the average ratio of Carbon to BGO inside the ball is 0.04 in volume and 8.5 x 10^{-6} in cubic radiation lenghts, with a resulting insignificant deterioration of the energy resolution. The 20 crates are held together by a metallic structure which allows the separation of the ball into two halves along a plane containing the ball axis. A special tool has been built to remove the crates individually from the ball. Any number of crates can be removed without affecting the position of the remaining crystals. In this way the BGO can be partially replaced with other types of detectors for special experiments.

d) Several photomultipliers have been tested and two have been selected to obtain the best compromise among efficiency, resolution, speed, linearity and cost. Appropriate voltage dividers have been designed.

e) Preliminary studies of the trigger and acquisition electronics have been completed. A reduced prototype of a linear fan-in and delay with 500 input channels is under costruction.

Detailed studies are now under way of the first experiments to be performed. As a gamma-ray calorimeter with a 2π symmetry around the beam axis, the ball is an ideal match for polarized gamma-ray beams as the one (Graal) under construction at the ESRF in Grenoble. This project will provide a beam of fully polarized and tagged gamma-ray

beam with a maximum energy of 1.5 - 2 GeV and an intensity around 10^7 photons per second. In a liquid Hydrogen target several centimeters long, this beam will produce some hundreds of pions, some η and some K^+ per second.

A new report discussing the different experimental possibilities opened by this apparatus at various laboratories is in preparation.

REFERENCES

1 P.Bernabei et al., Relazione alla Giunta INFN, unpublished;
A.Zucchiatti, Proceedings of the "*Workshop on Heavy-Quark Factory and Nuclear Physics Facility with Superconducting Linacs*", Courmayeur, 965, (1988);
A.Zucchiatti et al. Proceeding of the "*International Nuclear. Physics. Conference*" Sao Paulo 257, (1989).

2 A.Zucchiatti et al., Nucl. Instr. and Meth., **A281,** 341, (1989).

3 L.Adiels et al., Nucl. Instr. and Meth., **A244,** 380, (1986).

4 H.Dietl et al., Nucl. Instr. and Meth., **A235,** 464, (1985).

5 G.Blanar et al. "EPS Int. Conf. on High En. Phys". Lisbon 1981.

6 D.Williams, G.F.Snelling , J.Pickup, Nucl. Instr. and Meth., **39**, 141, (1966).

7 H.V.Piltingsrud,J. Nucl. Med., **20,** 1279, (1979).

8 F.Terzi Thesis Universit'a di Genova (1989) unpublished

9 C.Bernini et al., INFN/TC-89/13

10 S.A.Wender et al., Nucl. Instr. and Meth., **197**, 591, (1982);
M.Moszynski et al., Nucl. Instr. and Meth., **188**, 403, (1981).

11 C.Bernini Thesis Universita di Genova , (1989) unpublished

12 S.Bianco et al., Internal Report Università di Pavia FNT/PT-88/20

13 A.Drescher et al., Nucl. Instr. and Meth., **A249**, 277, (1986).

14 M.Schneegans, Nucl. Instr. and Meth., **A257**, 528, (1987).

15 R. Brun et al., GEANT3, CERN/DD/EE/84-1 (1987).